Bioorganic Chemistry 86 (2019) 61–79

Contents lists available at ScienceDirect

Bioorganic Chemistry

journal homepage: www.elsevier.com/locate/bioorg

Trifluoromethylated carboline compounds targeting DNA: Synthesis, binding and anti-proliferative effects on human cancer cell lines

Sarita Sarkar[a], Olga I. Shmatova[b], Valentine G. Nenajdenko[b], Kakali Bhadra[a,*]

[a] Department of Zoology, University of Kalyani, Nadia, West Bengal 741235, India
[b] Department of Chemistry, Lomonosov Moscow State University, Moscow 119991, Russia

ARTICLE INFO

Keywords:
Trifluoromethylated carboline compounds
Nucleic acid-small molecular binding
FTIR
ITC
Cell cytotoxicity
Apoptosis

ABSTRACT

Three sets of carboline derived compounds were prepared by Pictet-Spengler cyclization. These tetrahydro β- and γ-carbolines have CF_3 group with an additional amino alkyl chains (α- or δ-position) and guanidine alkyl chains (α-position), of varying length. Structure–activity relationship of these molecules with calf thymus DNA was emphasized by fluorescence, ITC, FTIR and viscosity. Binding with DNA resulted in dramatic enhancement and quenching in the fluorescence emission. Gamma-carboline analogs showed maximum DNA binding followed by beta-carboline compounds with amino alkyl chain and least with guanidine alkyl chain compounds. It decreased with increasing chain length. The bindings were entropically driven being more with guanidine alkyl chain analogs. Site preference and mode of binding with partial intercalation and external binding was supported by FTIR and viscosity. Cytotoxic potencies of the compounds were tested on seven different cancer cell lines. The smallest alkyl chain analog attached to gamma position, Comp3, showed maximum cytotoxicity with GI_{50} 6.2 μM, against HCT-116 causing apoptosis, followed by the guanidine alkyl chain compounds, but amino alkyl chain compounds to beta position showed poor cytotoxicity.

These results may be of prospective use in a framework to design novel carboline derivatives as antitumor drugs for improved therapeutic applications in future.

1. Introduction

Research in upcoming field of molecular medicine and gene therapy are constantly utilizing DNA as target macromolecules [1–3]. Hence, various classes of nucleic acid based drugs have evolved to a broad range of diseases including cancer and other genetic disorders, though most of these compounds are in early stages of clinical trials and research [4–8]. Most common chemotherapeutic agents are selective toxins and are more potent on rapidly proliferating normal cells, leading to extensive nonspecific side effects. Further, unlike other monogenetic diseases, cancer is a prime example of a disease process in which carcinogenic and metabolic changes are intertwined to promote cell survival and growth, hence mostly the drugs are non effective on all forms of cancer, which is again a very fundamental problem. Also, the basic mechanisms of action of these agents on specific target molecules are poorly understood.

Beta–carboline alkaloids (Fig. 1) are such a large group of natural and synthetic indole alkaloids, having myriad of proven therapeutic applications, including cancer and tumor treatment, hence numerous studies have been focused on their pharmacological effects [9–18]. Binding to nucleic acids of different motifs and antineoplastic ability for natural beta-carboline alkaloids were tested by several [16–19]. Furthermore, binding and antitumor activities of many synthetic beta-carboline derivative molecules were also analyzed before [20–22]. On the other hand, compared to beta-carbolines, interactive studies with gamma-carbolines are scanty [23–25]. Gamma-carbolines represent a structurally related class where the pyridine nitrogen is shifted by one position compared to beta-carbolines [23–25]. Though gamma-carbolines do not occur in nature, but few compounds have been studied as important drugs for anti-tumor (topoisomerase II inhibition), anti-allergic and potential anti-Alzheimer activity [23–25].

Three subsets of seven compounds, bearing CF_3 group (Fig. 2), with an additional amino alkyl (both at beta and gamma position) and guanidine alkyl chains, of varying length, to tetrahydro-carboline core, *viz.* trifluoromethylated analogues of natural alkaloids nazlinine, typargine and homotrypargines (Fig. 1), were prepared by Pictet-Spengler cyclization. These are starting point for the biosynthesis of several important alkaloid like compounds exhibiting a broad spectrum of biological activities but their anti cancer properties were never highlighted [26–29]. Further, fluorinated organic compounds are of special

* Corresponding author.
E-mail address: kakali_bhadra2004@yahoo.com (K. Bhadra).

https://doi.org/10.1016/j.bioorg.2019.01.028
Received 3 September 2018; Received in revised form 14 December 2018; Accepted 17 January 2019
Available online 18 January 2019

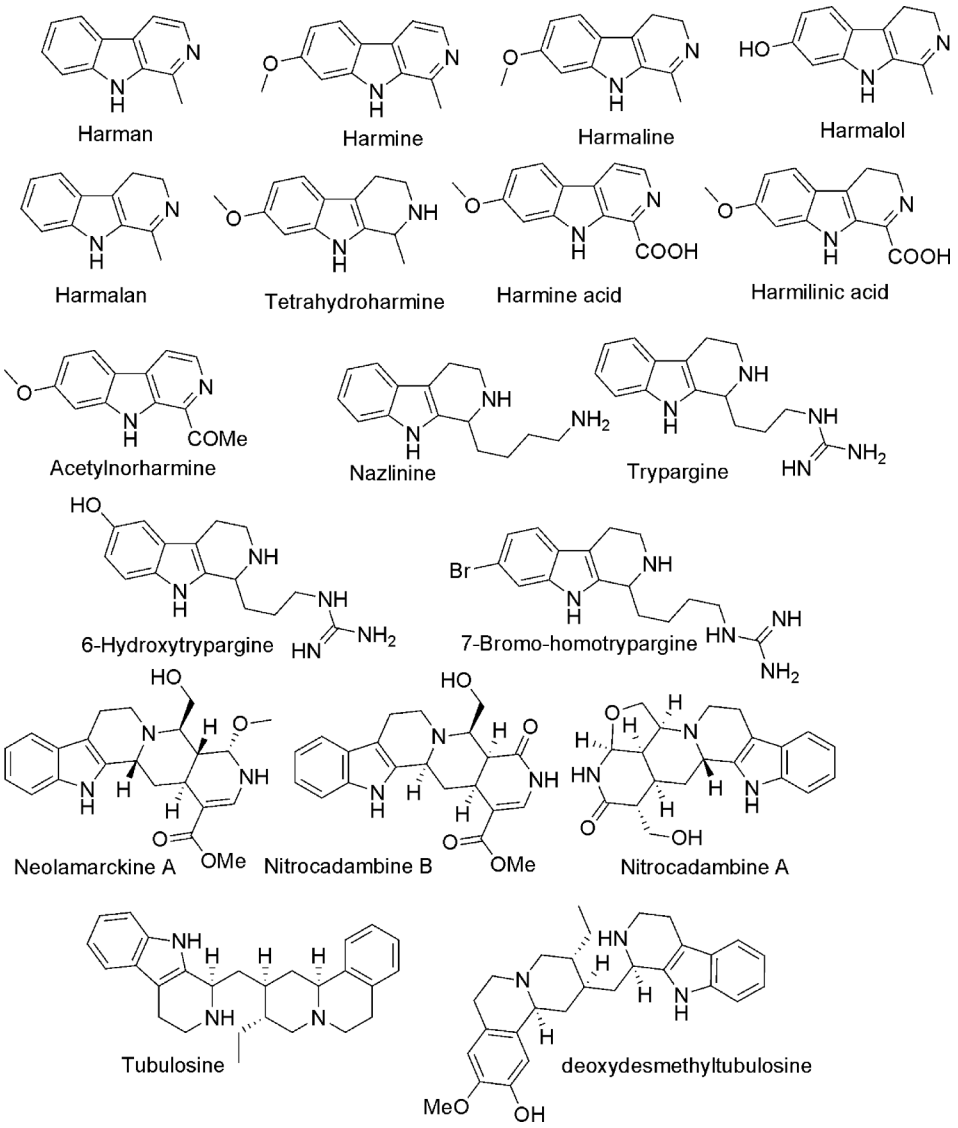

Fig. 1. Chemical structures of carboline alkaloids.

importance for modern material science and drug design. Incorporation of fluorine or the trifluoromethyl group in the target molecule is a useful modification in medicinal chemistry [30,31]. The two most important methods to prepare beta-carbolines are Pictet-Spengler reaction and Bischler-Napieralski reaction. These classical reactions are used to prepare tetrahydro (dihydro) isoquinoline derivatives from phenylethylamines and tetrahydro (dihydro) carbolines from tryptamines. Recently, few derivatives of nazlinine, trypargine and homotrypargine analogues having a trifluoromethyl group installed at the position 1 based on the use of alpha-trifluoromethylated cyclic imines as starting blocks have been reported by Shmatova *et al*, 2016 [27]. The incorporation of a CF_3-group (trifluoromethyl group) could significantly improve metabolic stability, lipophilicity and other physico-chemical properties of target molecules. Earlier, method for the synthesis of trifluoromethylated terahydrocarbolines elaborated by Nenajdenko and Haufe teams [26] used Pictet-Spengler approach, where CF_3-substituted enamines have been used as starting materials. However, except few [22] there are not much examples in the literature of synthesis, designing and biological significance of new carboline analogues with special focus on trifluoromethylated (CF_3) derivatives prepared by Bischler-Napieralski cyclization which will lead to the designing and development of small molecule based nucleic acid therapeutic agents in future.

This article for the first time describes in detail the binding, mode and mechanism of seven novel derivative molecules, bearing tetrahydro-carboline core group (Fig. 2), with DNA as biotarget, using fluorescence, ITC, viscosity and FTIR, in addition to its apoptotic induction ability in seven different cancer cell lines using different biochemical assays. Novelty lies in the fact that for the first time a comparative study of the two structural forms, beta and gamma-carbolines, related to DNA binding affinity and their efficacy as antitumor agent have been shown in this study. The synthetic compounds were subsequently screened for the best binding with potent anticancer activity following evidence of antineoplastic properties and inhibition of growth of a wide variety of tumor cells.

2. Materials and methods

2.1. Materials

Starting trifluoromethylated carbolines (Fig. 2) were prepared using the approach described recently by Shamatova *et al.,* 2016 [27]. The procedure for their preparation is based on Pictet-Spengler reaction of trifluoromethylated cyclic imines with tryptamines. This is a short and two steps synthesis of CF_3-derivatives of naturally occurring compounds (nazlinine, trypargine, homotrypargine). The method is highly

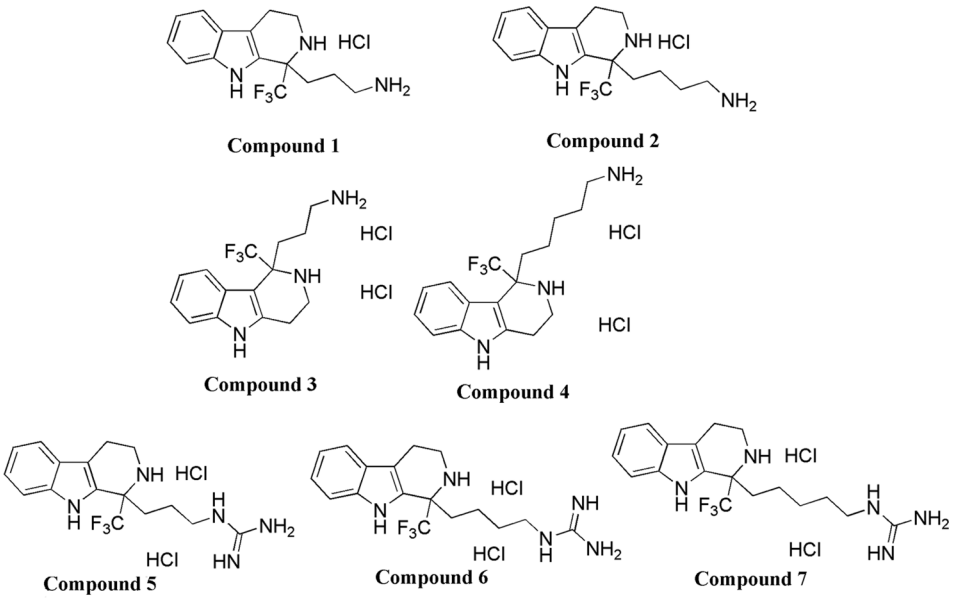

Fig. 2. Chemical structures of analog compounds bearing tetrahydro-carboline core group. Compound 1 and 2, beta-carboline analogs with amino alkyl chain, compound 3 and 4 are gamma-carboline analogs with amino alkyl chain and compound 5, 6 and 7 are beta-carboline analogs with guanidium alkyl chain.

efficient to prepare CF_3-substituted analogues of the carboline alkaloids in good or excellent yields.

CT DNA (Calf thymus DNA) was obtained from Sigma-Aldrich Corporation and used as such. Ethidium bromide and Hoechst 33,258 were purchased from Quest Chemicals, India. Concentrations were determined spectrophotometrically using molar extinction coefficient values of 5680 M^{-1} cm^{-1} and 4.2 × 10^4 M^{-1} cm^{-1} at 480 and 338 nm, respectively. All experiments were conducted in citrate-phosphate (CP) buffer (15 mM [Na^+]), pH 6.8, for studying the binding of the analog compounds to CT DNA.

Cancer and normal cell lines were obtained from NCCS (National Centre for Cell Science) Pune. Standard protocol as described earlier was used for the cell growth [32,33]. Seven different human cancer cell lines and one normal cell line *viz.* HeLa (cervical carcinoma), MDA-MB-231 (breast carcinoma), A549 (lung carcinoma), A375 (skin carcinoma), ACHN (kidney carcinoma), HCT116 (colon cancer cell line), $HepG_2$ (liver epitheloid carcinoma), HEK-293 (normal epithelial cells) and WRL-68 (normal hepatic cells) were chosen obtained from National Centre for Cell Science, Pune. Cells were grown in DMEM supplemented with 10% heat inactivated fetal bovine serum (FBS) and 1% antibiotic–antimycotic, in a humidified atmosphere at 37 °C with 5% CO_2. However for ACHN cell line, DMEM has been used as cell culture media.

2.2. Synthetic protocols

Carbolines were prepared according to the scheme as described in Scheme 1.

For n = 3

A tryptamine (160 mg, 1 mmol) was mixed with the 7-membered cyclic trifluoromethylated imine (0.165 g, 1 mmol) in CH_2Cl_2 (5 mL). Then trifluoroacetic acid (0.16 mL, 2.1 mmol) was added in one portion. The mixture remained at room temperature for 7 days, then diluted with CH_2Cl_2 (20–30 mL) and washed with saturated K_2CO_3 solution in a separating funnel. After drying over K_2CO_3 solvent was evaporated and pure substances were obtained.

For n = 1–2

An tryptamine (160 mg, 1 mmol) was mixed with the trifluoromethylated cyclic imines (**5**-membered – 0.137 g, 6-membered – 0.151 g, 1 mmol) and CSA (1.4 g, 6 mmol). In order to mix better the reactants we also added water (~3–5 mL). The reaction mixture was heated at 130 °C for 14 h on oil bath (the water evaporated during first 30 min, after which remaining black residue continues heating), then diluted with CH_2Cl_2 (20–30 mL) and washed with saturated K_2CO_3 solution in a separating funnel. After drying over K_2CO_3 the solvent was evaporated. The crude product was diluted with EtOH (1–2 mL), solution of oxalic acid dihydrate (0.126 g, 1 mmol) in EtOH (1–2 mL) was added. The resulting slurry was filtered through celite pad. Celite pad was washed with EtOH (~5–10 mL). The filtrate (about 10 mL) was evaporated, dissolved in the mixture of CH_2Cl_2 (20–30 mL) and saturated K_2CO_3 solution (20–30 mL). The organic phase was separated, dried over K_2CO_3 and evaporated.

To transform free bases to hydrochlorides the appropriate compound (1 mmol) was dissolved by methanolic hydrogen chloride (1 mL, 5 M) and then evaporated to dryness.

2.2.1. Synthesis of guanidine derivatives

An appropriate diamine (0.5 mmol), formamidinesulfinic acid (60 mg, 0.55 mmol) and triethylamine (1 mL) were dissolved in MeOH/H_2O. The mixture remained at room temperature overnight and the solvents were evaporated. The residue was diluted with CH_2Cl_2 (20–30 mL) and saturated K_2CO_3. The organic phase was separated, dried over K_2CO_3 and evaporated.

2.3. DNA binding studies

2.3.1. Spectroscopic analysis

Absorbance spectra were measured on a Jasco V-630 double beam monochromator spectrophotometer (Jasco International Co. Ltd. Tokyo, Japan) equipped with a thermoelectrically controlled cell holder in matched quartz cells of 1 cm path length under stirring at 25 ± 0.5 °C. Fluorescence spectra were obtained on a Hitachi F4010 fluorescence spectrometer (Hitachi Ltd., Tokyo, Japan) in fluorescence free quartz cells of 1 cm path length. According to the equation of Parker and Rees (1960) as described earlier [34], quantum yield calculations were made

$$\phi_s = (F_s \varepsilon_q C_q \times 0.55)/(F_q \cdot \varepsilon_s C_s) \quad (1)$$

where F is the integrated area of the fluorescence emission curve in

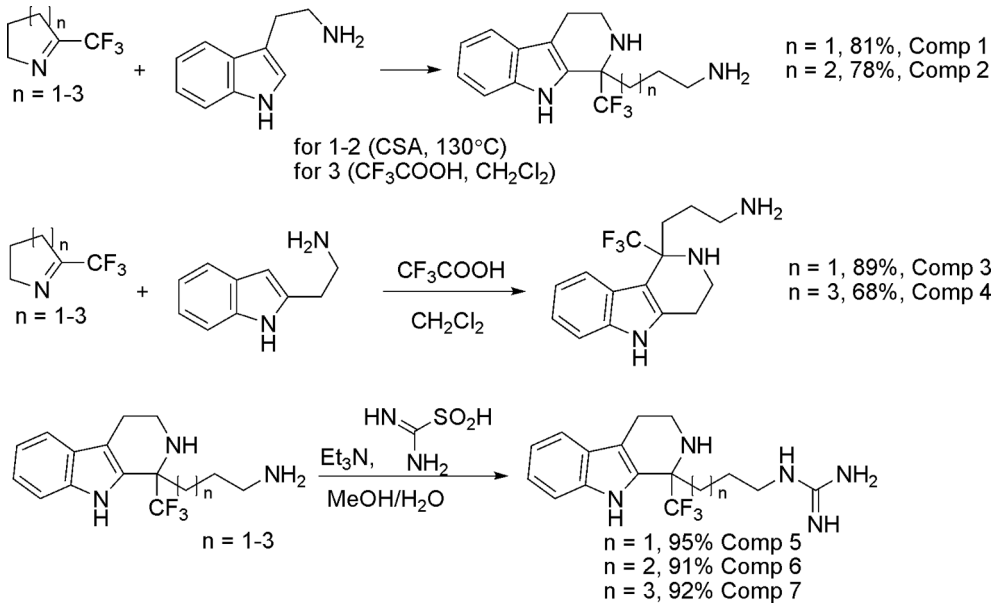

Scheme 1. Synthesis of carboline analog compounds.

arbitrary unit, ε represents the molar extinction coefficient and C represents the molar concentration of sample (s) and quinine sulphate (q) respectively. Quinine sulphate in 0.1 N H_2SO_4 was utilized as reference standard for quantum yield measurements.

2.3.2. Isothermal titration calorimetric (ITC) analysis of the binding

GE Microcal ITC 200 (Northampton, USA) and Origin 7.0 software was used for ITC measurements and analysis.

2.3.3. Solution viscometric study

Hydrodynamic study was performed by a Cannon-Manning Type 75 semi micro viscometer. Linear CT DNA was sonicated as described earlier [35,36]. After sonication, under sterile conditions the sample was extensively dialyzed against the buffer. Relative viscosities for nucleic acid in either the presence or absence of the analogs were calculated from the relation

$$\frac{\eta' sp}{\eta sp} = \frac{\left[\frac{tcomplex - t'o}{t'o}\right]}{\left[\frac{tcontrol - to}{to}\right]} \quad (2)$$

where η'_{sp} and η_{sp} are specific viscosities of the ligand-nucleic acid complex and the nucleic acid respectively, $t_{complex}$, $t_{control}$, t'_o and t_o are the average flow times for the complex, free nucleic acid, solvent for the complex and solvent for the free nucleic acid respectively.

2.3.4. FT-IR spectroscopic analysis

FT-IR experiments were recorded with a Perkin-Elmer Spectrum (Perkin Elmer, Inc, USA) to FT-IR spectrophotometers equipped with a diamond head attenuated total reflectance (ATR) accessory, $LiTaO_3$ detector and a KBr beam splitter at ambient temperature. For each spectrum 20 scans were collected at a resolution of 1 cm^{-1}. All the spectra were collected in 15 mM citrate phosphate buffer as a solvent (pH 6.8). All the spectra were collected in the range of 2300–600 cm^{-1} by averaging 20 scans with a resolution of 1 cm^{-1}. Background spectra are all collected with ZnSe before each measurement. All the spectra were baseline corrected and normalized for sharp band of CT DNA due to sugar C—C and C—O stretching vibrations at 968 cm^{-1} [19,37–39]. Similar intensity variations were used to determine the ligand binding to DNA bases in plane vibrations related to A-T, G-C base pairs and the PO_2 stretching vibrations such as 1714 (Guanine), 1662 (Thymine), 1608 (Adenine), 1490 (Cytosine) and 1227 cm^{-1} (PO_2 groups) [19,37–39]. To perform water subtraction, a spectrum of CP buffer was recorded and then subtracted from the spectra of free DNA and alkaloid-DNA complexes. A satisfactory water subtraction was achieved when the intensity of water combination band at about 2200 cm^{-1} became zero in the spectra of free DNA and ligand-DNA complexes [19,39]. FTIR of free DNA and all compounds were also recorded and subtracted from the spectra of drug-DNA complexes. This was done to make sure that the observed changes such as shift in peak position and intensity in the spectra of DNA were due to interaction with these compounds.

Preparation of stock solutions for FTIR. Appropriate amount of different compounds of beta-carboline with amino alkyl chain analogs (comp 1 and 2), gamma-carboline with amino alkyl chain analogs (comp 3 and 4) and beta-carboline with guanidine alkyl chain analogs (comp 5, 6 and 7) were dissolved in buffer and were added in drop wise to CT DNA solutions to prepare the desired drug (D) /DNA (P) molar ratios (*r*) of 1/10 and 1/15. The pH values of all complexes, DNA and drug solutions were adjusted at 6.8 ± 0.2. The infrared spectra were recorded after 1 h of mixing the respective compounds with DNA properly. DNA concentration of 3600 μM was used as fixed concentration.

2.4. In vitro cytotoxic assays

2.4.1. MTT assay

We tested the percentage of cell viability and calculated the GI_{50} (50% growth inhibition) values for the above mentioned cell lines by MTT (1 mg/ml of the tetrazolium dye and 3-(4,5-dimethylthiazol-2-yl)-2,5-diphenyltetrazolium bromide dissolved in phosphate buffer saline, pH 7.4) assay as reported earlier [32,33]. GI_{50} was calculated by using the equation

$$GI_{50} = (T - T_o) \times 100/(C - T_o) \quad (3)$$

where T is the optical density of the test well after 48 h drug exposure, T_o is the optical density at time zero & C is optical density of control. The experiment was repeated three times and average was taken.

2.4.2. FITC-Annexin V/PI FCM double staining

Double staining for FITC (fluorescein isothiocyanate) – Annexin V binding and for cellular DNA using PI (propidium iodide), FCM (flow cytometry) was performed as described by Mallick *et al* (2010) [40].

Table 1
Spectroscopic properties of free and bound trifluoromethyl derivative compounds with CT DNA.

Carboline compound	Molecular Weight	Melting point	IR peaks of free compound (1800–600 cm^{-1})	λ_{max}[a] (free)/nm	λ_{max}[a] of emission/nm	φ/φ_o at saturation P/D	ε_f (at λ_{max})/M^{-1} cm^{-1}	ΔTm °C at saturation D/P
A. Gamma-carboline with amino alkyl chain analog								
Compound 3; 3-(1-(Trifluoromethyl)-2,3,4,5-tetrahydro-1H-pyrido[4,3-*b*]indol-1-yl)propan-1-amine	297	Viscous compound	1436, 1407, 1313, 1016, 952, 702, 670	274	340	1.92;24	12,500	10.0
Compound 4; 5-(1-(Trifluoromethyl)-2,3,4,5-tetrahydro-1H-pyrido[4,3-*b*]indol-1-yl)pentan-1-amine	325	Viscous compound	1435, 1404, 1312, 1018, 953, 701, 669	274	343	1.85;28.5	11,000	8.5
B. Beta-carboline with amino alkyl chain analog								
Compound 1; 3-(1-(Trifluoromethyl)-2,3,4,9-tetrahydro-1H-pyrido[3,4-*b*]indol-1-yl)propan-1-amine	297	89–91 °C	1741, 1705, 1585, 1461, 1385, 1254, 1156, 1076, 955, 805, 734, 687, 639	277	350	0.31;42	8790	7.5
Compound 2; 4-(1-(Trifluoromethyl)-2,3,4,9-tetrahydro-1H-pyrido[3,4-*b*]indol-1-yl)butan-1-amine	311	116–118 °C	1734, 1688, 1628, 1553, 1460, 1384, 1251, 1155, 1077, 1002, 968, 803, 737, 707, 636	277	350	0.40;50	9000	7.5
C. Beta-carboline with guanidine alkyl chain analog								
Compound 5; 1-(3-(1-(Trifluoromethyl)-2,3,4,9-tetrahydro-1H-pyrido[3,4-*b*]indol-1-yl)propyl) guanidine	339	117–119 °C	1767, 1436, 1404, 1326, 1022, 952, 697, 671	274	351	1.59;62	9000	3.0
Compound 6; 1-(4-(1-(Trifluoromethyl)-2,3,4,9-tetrahydro-1H-pyrido[3,4-*b*]indol-1-yl)butyl) guanidine	353	106–108 °C	1750, 1600, 1434, 1401, 1313, 1021, 952, 698, 665	274	352	1.53;70	10,400	3.0
Compound 7;1-(5-(1-Ttrifluoromethyl)-2,3,4,9-tetrahydro-1H-pyrido[3,4-*b*]indol-1-yl)pentyl) guanidine	367	85–87 °C	1433, 1312, 1022, 951, 699	274	352	1.32;84	12,000	2.0

[a] Units: λ nm, ε (molar extinction coefficient), M^{-1} cm^{-1}; ΔTm °C = $T_m - T_o$ (67 °C for native CT DNA at 15 mm of CP buffer).

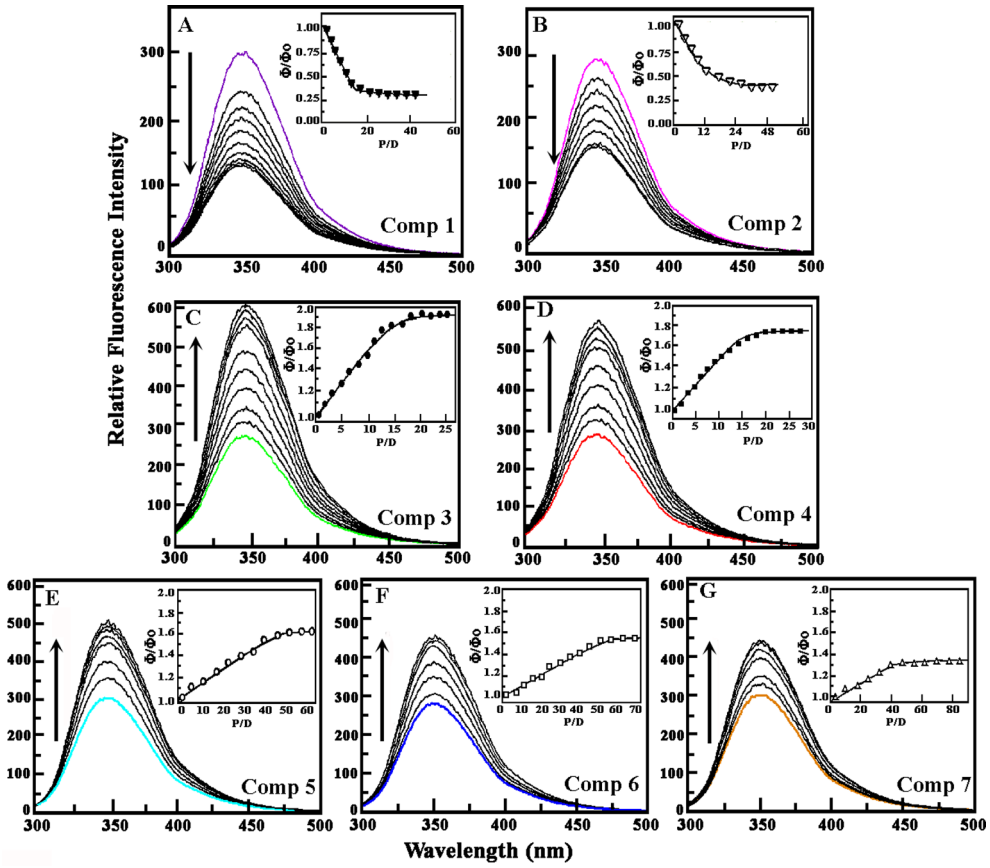

Fig. 3. Steady state fluorescence emission spectrum of the analog compounds 1–7 (2.5 μM each, in coloured spectra) treated with various concentrations of CT DNA in 15 mM CP buffer, pH 6.8 at 25 ± 0.5 °C. Inset of A-G represent plots of the relative quantum yield φ/φ_o versus P/D for the interaction of the compounds with CT DNA. The quantum yield values have been described in Table 1.

2.4.3. Scanning electron microscopy

To study the external morphology of cell, they were first fixed in glutaraldehyde and dehydrated through a graded series of ethanol. Subsequently, they were cleaned in tetrachloromethane, air-dried and coated with gold in IB2 ION COATER and observed using S530 Hitachi scanning electron microscope.

2.4.4. Transmission electron microscopy

After sample preparation as described earlier [33], the samples were finally observed using TECNAI 200KV TEM (Fei Electron Optics), 35 mm Photography System from All India Institute of Medical Science, N. Delhi.

2.4.5. Comet assay

Single cell gel electrophoresis or Comet assay was performed on isolated HCT-116 cells reported earlier. Comet tail length, using the software Casp, gives a measurement of extent of DNA damage.

2.4.6. Cell cycle analyses

Cell cycle inhibition analyses of comp3 (3, 6.2 and 9 μM) treated HCT116 (grown at a density of 2×10^5 cells/ml in 70 mm culture plate) were analyzed using PI (propidium iodide) staining.

2.4.7. Immunofluorescence

Anti active caspase 3 monoclonal primary antibody (17 Kd, Santa Cruz Biotechnology), anti p53 monoclonal primary antibody (Santa Cruz Biotechnology) and anti-mouse secondary antibody (FITC tagged, Sigma) were used. HCT116 cells were first grown on cover slips and after getting 70–80% cell confluency the cells were treated with comp 3 with concentration of 3, 6.2 and 9 μM, respectively. The cells were then washed with cold PBS, fixed with 4% paraformaldehyde, washed again and incubated with 0.1% Triton X-100. Cells were then blocked with 5% BSA in TBS and incubated with appropriate primary antibodies (activated caspase 3 and p53) in 1% bovine serum albumin at 4 °C. After that cells were again washed with TBS and incubated with an appropriate fluorescence-conjugated secondary antibody at room temperature. Finally, the cells were washed, counter stained with DAPI, mounted on a glass slide and observed under a confocal microscope and was subsequently analyzed.

3. Results and discussion

The study focused on the interaction of seven synthetic tetrahydro -carboline compounds *viz.* compound 1 and 2 (beta-carboline analogs with amino alkyl chain), compound 3 and 4 (gamma-carboline analogs with amino alkyl chain) and compound 5, 6 and 7 (beta-carboline analogs with guanidium alkyl chain), respectively, with CT DNA (Calf thymus DNA) along with the anti proliferative and apoptotic induction ability of the analogs on seven cancer cell lines *viz.* HeLa, MDA-MB-231, A549, A375, ACHN, HCT-116 and $HepG_2$.

3.1. Interaction of carboline compounds with CT DNA

3.1.1. Spectroscopic analysis

UV Spectroscopic study of the analogs at pH 7.0 exhibits λ_{maxima} at 277 nm for compound 1 and 2, while, for compound 3, 4, 5, 6 and 7, at 274 nm, respectively. λ_{maxima} of all the analogs were very close to DNA λ_{maxima} peak (260 nm), hence U.V spectroscopic titration analysis (to calculate the binding constant values and stoitiometry) was avoided. However, results from optical melting experiments revealed stabilization of the CT DNA after interaction with all the compounds (Figure not shown). The native melting temperature of CT DNA (67 °C) at 15 mM was stabilized to 74.5 ± 0.5 °C in presence of compound 1 and 2, 77 ± 0.5 °C with compound 3, 75.5 ± 0.5 °C with compound 4, 70 ± 0.5 °C with compound 5, 70 ± 0.5 °C with compound 6 and least with compound 7, only 69 ± 0.5 °C, respectively. Summary of the

optical properties of free and bound beta and gamma-carboline analogs with CT DNA have been collated in Table 1. High stabilizing melting temperature of the complex was assumed to be due to intercalated or partially intercalated binding of the analog while low melting stabilization signify groove or superficial binding of the compound, though it is not a confirmatory analysis.

Furthermore, the strong fluorescence spectra of the analog compounds provide a suitable tool to observe the interaction phenomena. Table 1 summarizes the emission spectral peak of all the seven analogs that varies from 340 to 352 nm when exited at 280 nm showing their respective strong fluorophoric nature. Fluorescence emission spectra of the synthetic compounds on titration with CT DNA showed both enhancement (compound 3, 4, 5, 6 and 7) and quenching (compound 1 and 2) of varying percent and it was recorded in the range of 300–500 nm (Fig. 3A–G). Percent enhancement of fluorescence with compound 3 was found to be 73% reaching saturation at P/D 24, with compound 4 it was observed to be 68% at P/D 28.5, with compound 5 it was observed to be 58% at P/D 62, with compound 6 it was analyzed to be 55% at P/D 70 and least with compound 7 (50%) at P/D 84, respectively, without any noticeable shift in the wavelength maximum. While, with compound 1 and 2, 64% and 60% quenching at P/D 42 and 50, respectively, was recorded. The phenomena of progressive increase and decrease of fluorescence intensity of the ligand in presence of nucleic acids, is basically due to strong interaction, which is still a controversial issue [41,42]. Considering these progressive trend of decrease in percent enhancement and quenching it may be inferred that the interaction of the analogs with CT DNA varied in the order of compound 3 > compound 4 > compound 1 > compound 2 > compound 5 > compound 6 > compound 7. Further, the quantum yield ϕ/ϕ_o values of the analog complexes with the DNA were also analyzed and presented in Table 1.

3.1.2. Thermodynamic characterization of analog compounds-CT DNA complex

In addition to the spectroscopic characterization of the interaction, we present new insights in terms of thermodynamics of the interaction. The binding affinity values of the analog compounds with CT DNA at 25 ± 0.5 °C were evaluated from the ITC (Isothermal calorimeter) data (Table 2). ITC is a responsive and consistent methodology for the direct measurement of thermodynamic parameters in various biomolecular interactions [43–45]. Previously, Yang *et al.*, 1994 and Du *et al.,* 2004 reported the thermodynamic parameters for the interaction of carboline derivatives with DNAs [46,47]. The derivative compounds, due to its high heat of dilution and aggregation tendency, a reverse protocol have been adopted. The bindings were exothermic and entropically driven in all the cases, though the extent varies (Fig. 4A–F, Table 2). Binding constant, K_b of 11.36 ± 0.15 × 10^5 M^{-1} with a stoichiometry of 6.5 nucleotide phosphates was observed for compound 3 and K_b of 7.96 ± 0.01 × 10^5 M^{-1} with a stoichiometry of 7.0 for compound 4 were analyzed for the gamma-carboline amino alkyl chain compounds with CT DNA. Further, K_b of 6.15 ± 0.01 × 10^5 M^{-1} with a stoichiometry of 8.0 for compound 1 and K_b of 4.70 ± 0.03 × 10^5 M^{-1} with a stoichiometry of 8.0 with compound 2 were calculated for the beta-carboline amino alkyl chain compounds with CT DNA. While, CT DNA with the analogs of guanidium alkyl chain compounds, showed K_b of 2.10 ± 0.02 × 10^5 M^{-1} with a stoichiometry of 8.5 for compound 5, K_b of 1.94 ± 0.03 × 10^5 M^{-1} with a stoichiometry of 8.7 with compound 6 (figure not shown) and K_b of 0.84 ± 0.05 × 10^5 M^{-1} with a stoichiometry of 10 with compound 7, respectively. Furthermore, other thermodynamic parameters like enthalpy change (ΔH^o), entropy contribution ($T\Delta So$) and free energy change (ΔG^o) are also presented in Table 2 and Fig. 4. Generally large negative enthalpy change was observed for intercalative interaction of small molecules to nucleic acids [48]. However interaction of DNA with the above synthetic compounds were all entropically driven with either moderate or very low enthalpy change, signifying partial intercalation or surface binding. The enthalpy change (ΔH^o) for compound 3 and 4 (gamma-carbolines with amino alkyl chain analogs) were −3.10 ± 0.02 and −2.69 ± 0.01 kcal/mol, respectively. While compound 1 and 2 (beta-carbolines with amino alkyl chain analogs) showed −2.60 ± 0.01 and-2.40 ± 0.03 kcal/mol and with compound 5, 6 and 7 (beta-carbolines with guanidine alkyl chain analogs) enthalpy change (ΔH^o) of −0.55 ± 0.02, −0.45 ± 0.02 and −0.25 ± 0.02 kcal/mol was observed. The bindings were entropically driven being more with guanidine alkyl chain analogs (6.75, 6.80 and 7.00 kcal/mol for compound 5, 6, and 7 respectively) than the amino alkyl chain analogs (5.21, 5.40, 5.30, 5.38 kcal/mol for compound 3, 4, 1 and 2, respectively). Large entropically driven bindings are suggestive of the disruption and release of water molecules [36,49]. Weak affinity with entropy driven binding in guanidine alkyl chain analogs is probably due to more stabilized and delocalization of the charge on the large guanidinium ion. Free energy change (ΔG^o) analyzed from the interaction lies between −6.5 to −8.5 kcal/mol. The overall variations of thermodynamic profiles for CT DNA binding to the seven analog compounds have been presented graphically in Fig. 5 to visualize the differences.

Table 2
ITC derived binding and thermodynamic profiles at 25 ± 0.5 °C for the interaction of calf thymas DNA (CT DNA) to different trifluoromethyl derivative compounds.[a]

carboline compounds	K_b(×$10^5$$M^{-1}$)	N	ΔG^o (kcal/mol)	ΔH^o (kcal/mol)	$T\Delta So$ (kcal/mol)
A. Gamma-carboline with amino alkyl chain analog					
Comp 3	11.36 ± 0.15	6.5	−8.31 ± 0.03	−3.10 ± 0.02	5.21
Comp 4	7.96 ± 0.01	7.0	−8.09 ± 0.04	−2.69 ± 0.01	5.40
B. Beta-carboline with amino alkyl chain analog					
Comp 1	6.15 ± 0.01	8.0	−7.90 ± 0.04	−2.60 ± 0.01	5.30
Comp 2	4.70 ± 0.03	8.0	−7.78 ± 0.03	−2.40 ± 0.03	5.38
C. Beta-carboline with guanidine alkyl chain analog					
Comp 5	2.10 ± 0.02	8.5	−7.30 ± 0.04	−0.55 ± 0.02	6.75
Comp 6	1.94 ± 0.03	8.7	−7.25 ± 0.05	−0.45 ± 0.02	6.80
Comp 7	0.84 ± 0.05	10	−6.75 ± 0.03	−0.25 ± 0.02	7.00

[a] Average of three determinations in CP Buffer, pH 6.8. Values of ΔG^o were determined using the equation $\Delta G^o = -RT \ln K_b$ and $T\Delta So = \Delta H^o - \Delta G^o$. N denotes the binding site size.

3.1.3. FT-IR analysis

Infrared (IR) spectra of free form of seven different compounds (*vide supra*), ethidium bromide and Hoechst 33,258 have been recorded in the range of 1800–600 cm^{-1} (Fig. 6). The infrared spectral features observed in CT DNA, of the free and complex form due to its interaction with seven different synthetic compounds *viz.* beta-carboline with amino alkyl chain analog (comp1 and comp2), gamma-carboline with amino alkyl chain analog (comp3 and comp4), beta-carboline with guanidine alkyl chain analog (comp5, 6 and 7) have been shown in Fig. 7 and compared with the spectral feature with Ethidium bromide (as classical intercalator) and Hoechst 33,258 (as groove binder).

Phosphate (PO_2) stretching vibrations (symmetric and asymmetric), deoxyribose sugar stretching of phosphate sugar backbone and ring vibrations of nitrogenous bases (C═O, C═N stretching) of DNA are confined from 1800 cm^{-1} to 600 cm^{-1} infrared region. In the infrared spectrum of free form of CT DNA, bands arise at 1223 and 1086 cm^{-1} and due to the vibration caused by phosphate asymmetric and symmetric stretching respectively. Deoxyribose sugar vibrations due to C = 0 and C—C stretching is denoted by IR bands at 1051 and 967 respectively in the free CT DNA. The IR band at 837 is primarily attributed to the vibrations of phosphodiester bonds. Other bands at 1370, 1295,779 and 727 cm^{-1} are attributed to sugar conformations. The band at 1712 cm^{-1} is due to the plane vibrations of guanine (G) stretching, the band at 1650 cm^{-1} is attributed primarily to thymine

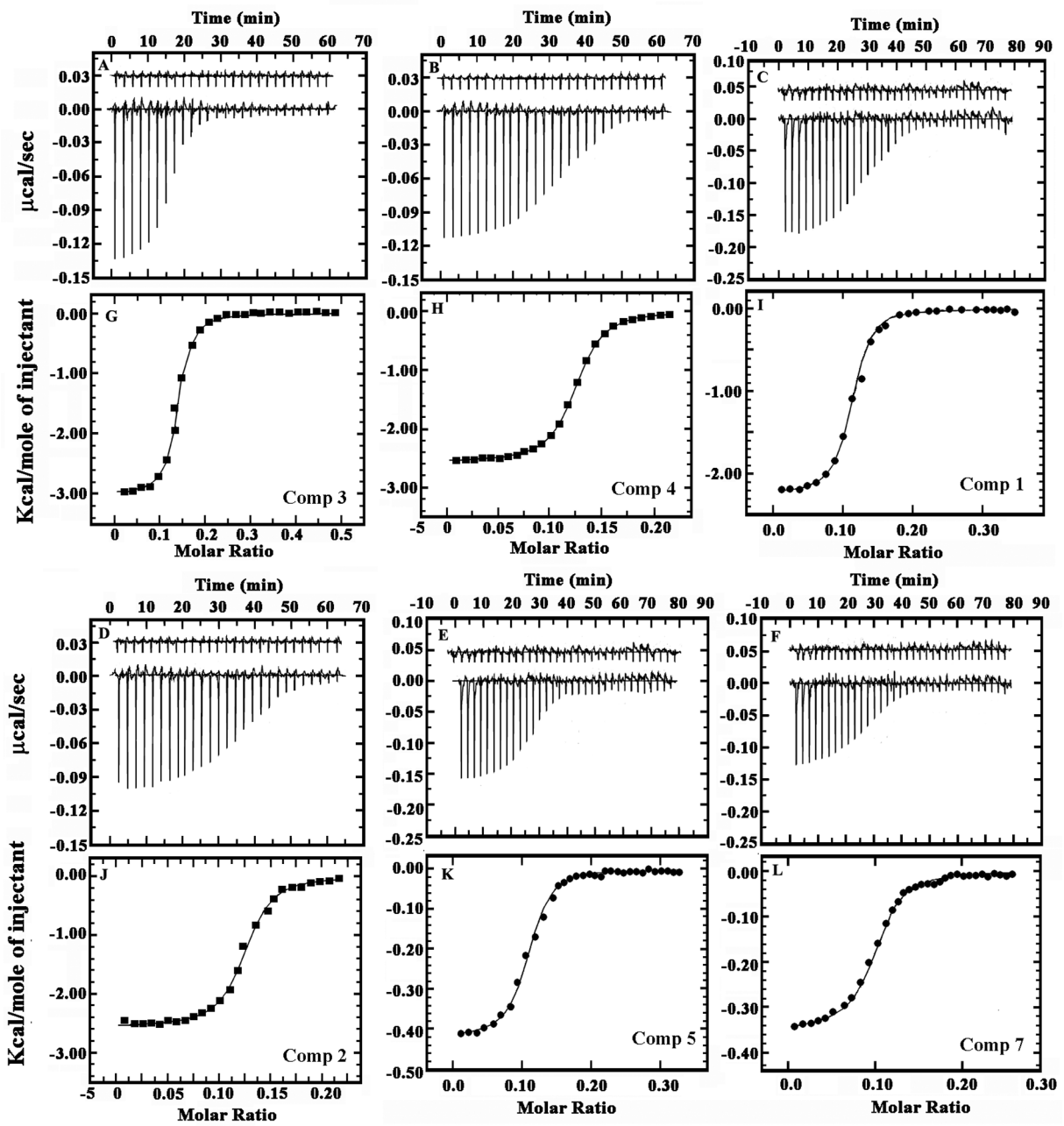

Fig. 4. ITC profile for the binding of 1500 µM of CT DNA to carboline analog compounds (15 µM each) at 25 ± 0.5 °C, pH 6.8 for (A–F). Each heat burst curve (in the bottom part of upper panel) is the result of a 1.5 µL sequential injection of the DNA into drug (curves at the bottom). The top part of upper panel show the heat burst for the injection of the DNA into the same buffer as control in each experiment (curves offset for clarity). The lower panel represent the corresponding normalized heat data against the molar ratio (P/D) (G, H, I, J, K and L). The data points (●-● and ■-■) reflect the experimental injection heats while the solid line represents the calculated best fit of the data. The values of the various thermodynamic parameters obtained are presented in Table 2.

(T) stretching vibrations, the bands at 1608 cm^{-1} and 1490 cm^{-1} appear due to the ring stretching vibrations of adenine (A) and cytosine (C) respectively and the band emerges at 1521 cm^{-1} is assigned to the plane stretching vibrations of guanine and cytosine residues [19,40]. Shifts in band position for the nitrogenous bases of DNA are also accompanied by the changes in intensities at the molar ratios (*r*) *viz.* 1/10 and 1/60, of the respective compound-DNA complexes. Furthermore, difference spectra of compound-DNA complexes [(DNA solution + compound solution)-DNA solution] have been shown in Fig. 8.

IR band observed in the free DNA at 1712 cm^{-1} for G shows 2 cm^{-1} increment in both 1/10 and 1/60 M ratios with comp1 and comp 2, while for comp 3-DNA complex the band at 1712 cm^{-1} shows 3 and 5 cm^{-1} increment, comp 4 and comp 5 shows 2 and 3 cm^{-1} increment, comp 6 shows 1 cm^{-1} increment and 2 cm^{-1} downshift at both the molar ratios while comp 7 shows no increment and downshift at 1/60 and 1/10 M ratios. No shift at 1650 cm^{-1} has been found for comp1 after the formation of complex with CT DNA for T stretching vibration at both 1/10 and 1/60 M ratios, while slight downshift of 1 and 2 cm^{-1} has been observed for comp2, remarkable changes of 2 cm^{-1} and 5 cm^{-1} downshift at 1650 cm^{-1} have been observed with comp3, 2 cm^{-1} downshift has been found for comp4, 3 cm^{-1} and 4 cm^{-1} downshift at 1650 cm^{-1} have been observed for comp5 and comp7, while 2 cm^{-1} upshift at 1650 cm^{-1} has been observed for comp6 at both the molar ratios. IR band observed at 1490 cm^{-1} of free CT DNA also shows minor downshifts to 1488 cm^{-1} at both the molar ratios for comp1, while no observable change or shift at 1490 cm^{-1} has been

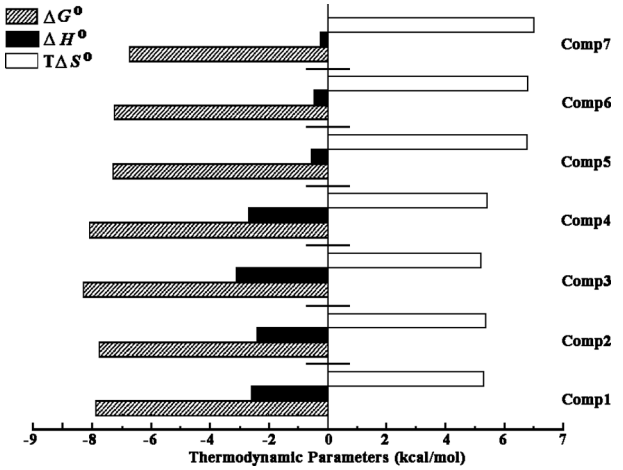

Fig. 5. Overall thermodynamic profiles for the binding of analog compounds 1–7 to CT DNA determined from ITC analysis at 25 ± 0.5 °C.

found for comp2, comp4, comp5, comp6 and comp7 interacting with DNA, whereas interaction with comp3 shows major upward shifts to 1499 cm^{-1} and 1497 cm^{-1} at 1/60 and 1/10 M ratios, respectively. The band at 1521 cm^{-1} assigned to stretching vibrations of G-C residues show very little down shift to 1520 cm^{-1} and 1519 cm^{-1} at both the molar ratios in case of Comp1 with CT DNA, while no shift has been found for comp2, whereas comp3 shows major upward shift to 1530 cm^{-1} at both 1/60 and 1/10 M ratios, comp 4 shows minor upward shift to 1523 cm^{-1}, very little down shifting of 1 cm^{-1} at 1/10 M ratios has been found with comp5, while with comp6 and comp7 no changes in shifting have been reported at both the molar ratios. No shift has been found in the band of adenine at 1608 cm^{-1} in comp1, comp2, comp4, comp5, comp6 and comp7 interacting with DNA at both molar ratios, while 2 cm^{-1} downshift has been reported for comp3 at both the molar ratios. Minor decrease in the intensity of bases bands have been found in case of comp1 and comp2 interacting with DNA and this can be related to moderate stabilization of DNA, while major increase in shifting and decrease in the intensity of bases bands have been observed in case of comp3-DNA complex revealing strong stabilization of DNA. Again with comp 4 slight increase in shifting and decrease in the intensity of bases bands have been found, where as no remarkable increase in shifting and decrease in the intensity of bases bands have been found with comp 5, 6 and 7. The stabilizing properties of these compounds with CT DNA was also analyzed by UV melting (*vide supra*, Table 1) and they showed the same trend as observed in FTIR.

Slight spectral changes (intensity and shifting) have been observed at phosphate asymmetric and symmetric bands for comp 1 and comp2 while, major spectral changes have been observed for comp3, comp4, comp5, comp6 and comp7 binding with CT DNA. Slight upward shift has been found to 1224 cm^{-1} and 1226 cm^{-1} at 1/60 and 1/10 M ratios for comp1, while an upward shift to 1225 cm^{-1} has been observed for comp2 at 1/10 M ratio, slight upward shift from 1223 cm^{-1} to 1228 cm^{-1} and 1232 cm^{-1} have been reported for comp3, an upward shift from 1223 cm^{-1} to 1229 cm^{-1} and 1230 cm^{-1} has been observed for comp4, an upward shift from 1223 cm^{-1} to 1226 cm^{-1} and 1235 cm^{-1} for comp5, slight downward shift has been found from 1223 cm^{-1} to 1221 cm^{-1} for comp6 and a slight upward shift has been observed from 1225 cm^{-1} to 1227 cm^{-1} for comp7. 1 and 2 cm^{-1} downshift has been observed at symmetric phosphate band at 1086 cm^{-1} to 1085 and 1084 cm^{-1} at both the molar ratios for comp1 and comp2, whereas 1 cm^{-1} downshift and a major intensity loss has been observed at symmetric phosphate band at 1086 cm^{-1} to 1085 cm^{-1} for comp3, 1 cm^{-1} downshift and a huge intensity loss has been observed at symmetric phosphate band at 1086 cm^{-1} to 1085 and 1083 cm^{-1} for comp4, 2 cm^{-1} and 6 cm^{-1} downshift and huge

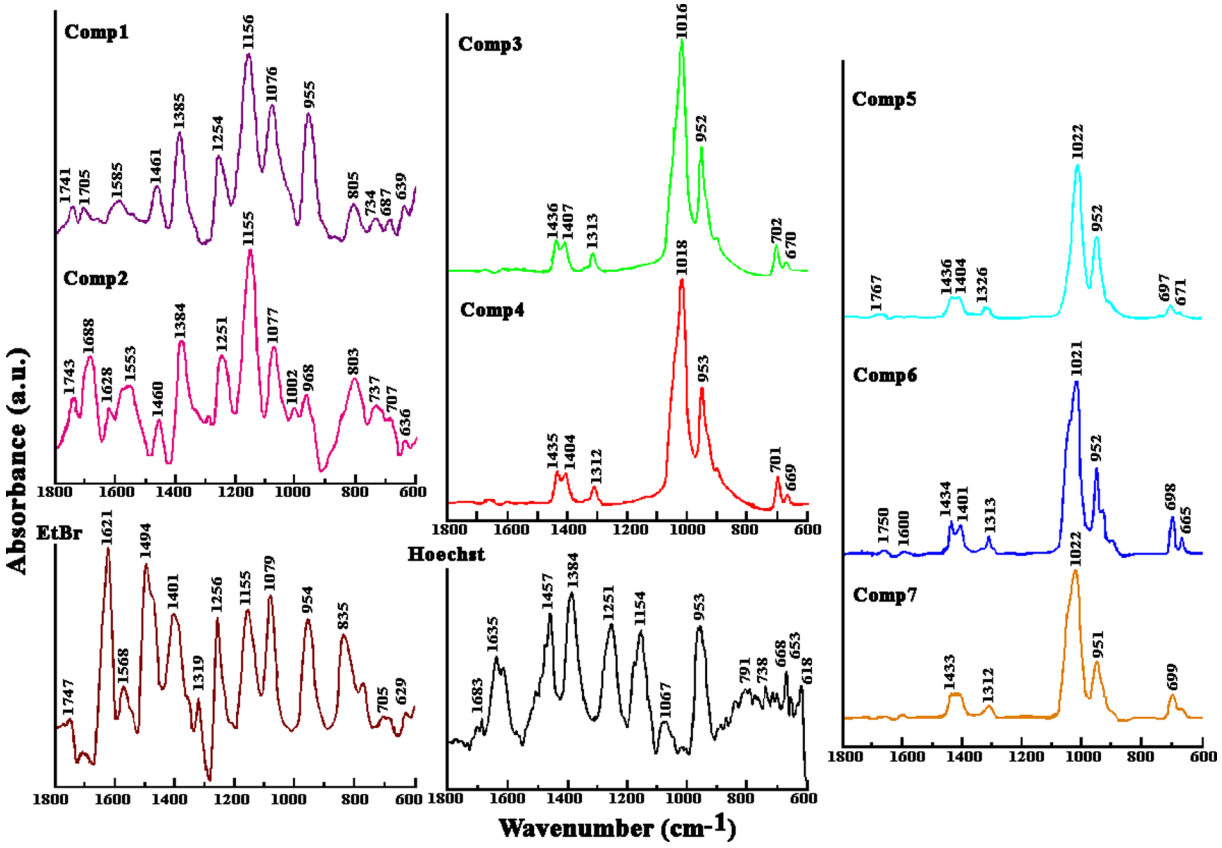

Fig. 6. FTIR spectra of seven analog compounds, Ethidium bromide and Hoechst 33,258 recorded in the range of 1800–600 cm^{-1}.

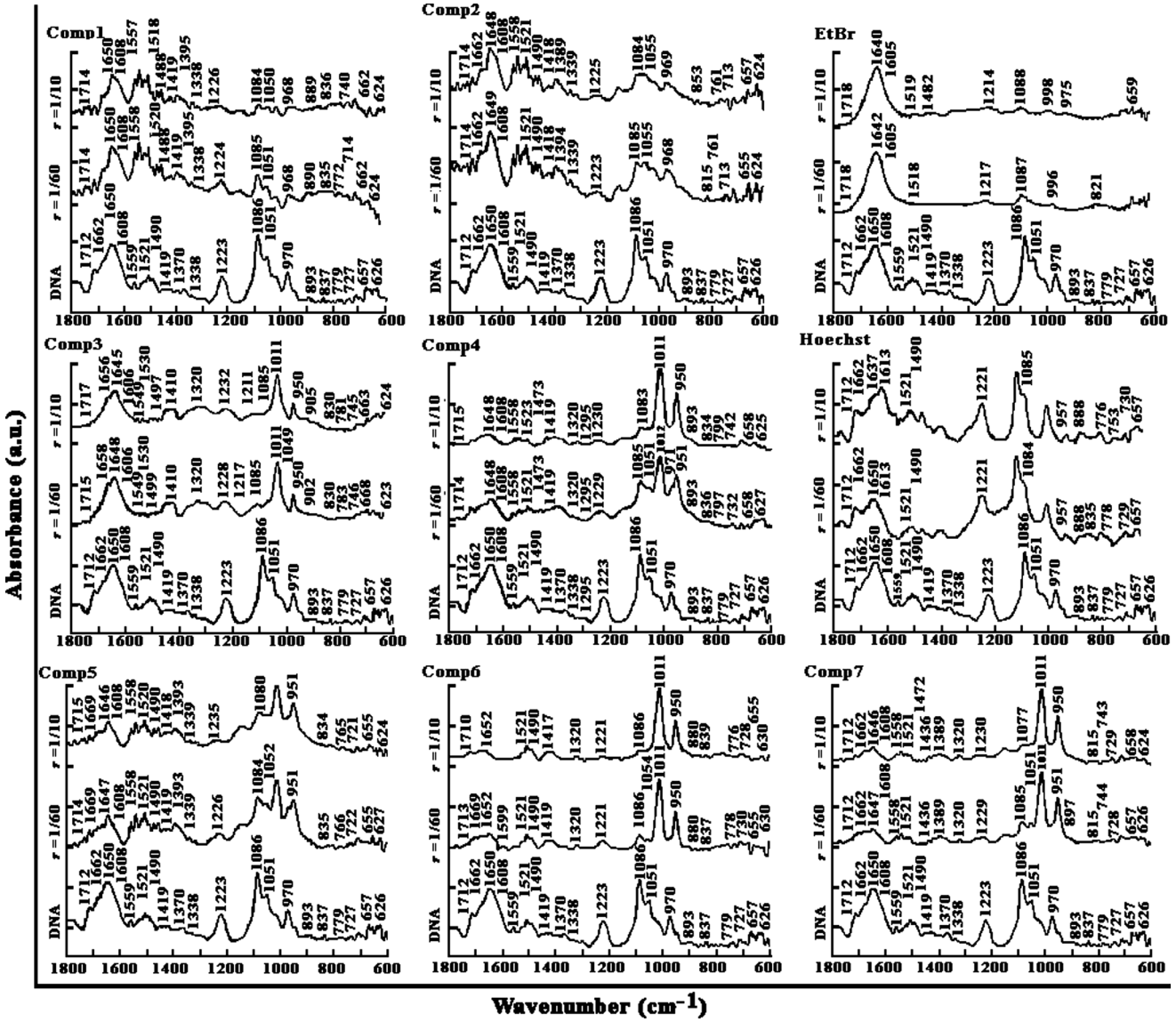

Fig. 7. Comparison of FTIR spectra of free CT DNA and complexation with analog compounds, ethidium bromide and Hoechst 33,258 at different molar ratios r 1/60 and 1/10 respectively.

intensity loss has been observed at symmetric phosphate band at 1086 cm^{-1} to 1084 and 1080 cm^{-1} for comp5 indicating variations in intensity of phosphate asymmetric and symmetric vibrations, huge intensity loss has been observed at symmetric phosphate band at 1086 cm^{-1} for comp6 and 1 cm^{-1} and 9 cm^{-1} downward shifting and intensity loss have been observed at both the molar ratios with comp7. No shifting has been observed at the IR band of 1051 cm^{-1} of free CT DNA with comp1, while 4 cm^{-1} upward shifting has been found at the IR band of 1051 cm^{-1} with comp 2 which attributes slight external binding due to deoxy sugar vibrations for C═O and C–C stretching, minor downward shifting of 2 cm^{-1} with a huge decrease in intensity has been observed with comp3, huge decrease in intensity has been observed for comp4, comp5, comp6 and 7 at the IR band of 1051 cm^{-1} at 1/60 M ratios with an upward shift of 1 cm^{-1} and 3 cm^{-1}, respectively for comp 5 and comp6. Slight downshift of 2 cm^{-1} and 1 cm^{-1} has been observed for comp 1 and comp 2 from 837 cm^{-1} to 835 cm^{-1} and 836 cm^{-1} at 1/60 and 1/10 M ratios due to slight interaction with CT DNA backbone. Major downshift of 7 cm^{-1} has been observed with comp3 from 837 cm^{-1} to 830 cm^{-1} at both the molar ratios due to the interaction and external binding with CT DNA backbone whereas, minor downshift of 1 cm^{-1} and 3 cm^{-1} has been observed for comp4 from 837 cm^{-1} to 836 and 834 cm^{-1}, while minor downshift of 2 and 3 cm^{-1} has been observed with comp 5 from 837 cm^{-1} to 835 and 834 cm^{-1}, minor upward shift of 2 cm^{-1} has been observed with comp6 from 837 cm^{-1} to 839 at 1/10 M ratios due to the slight interaction with CT DNA backbone and with comp7 no shifting has been found at 837 cm^{-1} due to the very poor interaction with CT DNA backbone. Maximum upward shifting from 779 cm^{-1} to 783 cm^{-1}, attributing to sugar conformation due to the interaction between comp3 with CT DNA, takes place, while with comp 4 maximum upward shifting from 727 to 732 cm^{-1} has been found, minimum downward shifting from 779 cm^{-1} to 766 cm^{-1} and 765 cm^{-1} at 1/60 and 1/10 M ratios has been reported for comp5, minimum upward shifting from 727 cm^{-1} to 730 cm^{-1} and 728 cm^{-1} has been reported for comp6 and minimum upward shifting from 727 cm^{-1} to 728 cm^{-1} and 729 cm^{-1} at both the molar ratios takes place for comp 7 binding to CT DNA.

From all the observed peak shifting and changes in intensity, it can be revealed, a very weak interaction of comp 1 to G and C while comp 2 showed slight interaction with bases G and T though they are both beta-carboline compounds with amino alkyl chain analogs, but the gamma-carboline with amino alkyl chain analog, comp 3, interacts maximum with G,C, G-C and very less with T, while, comp 4 on interaction with

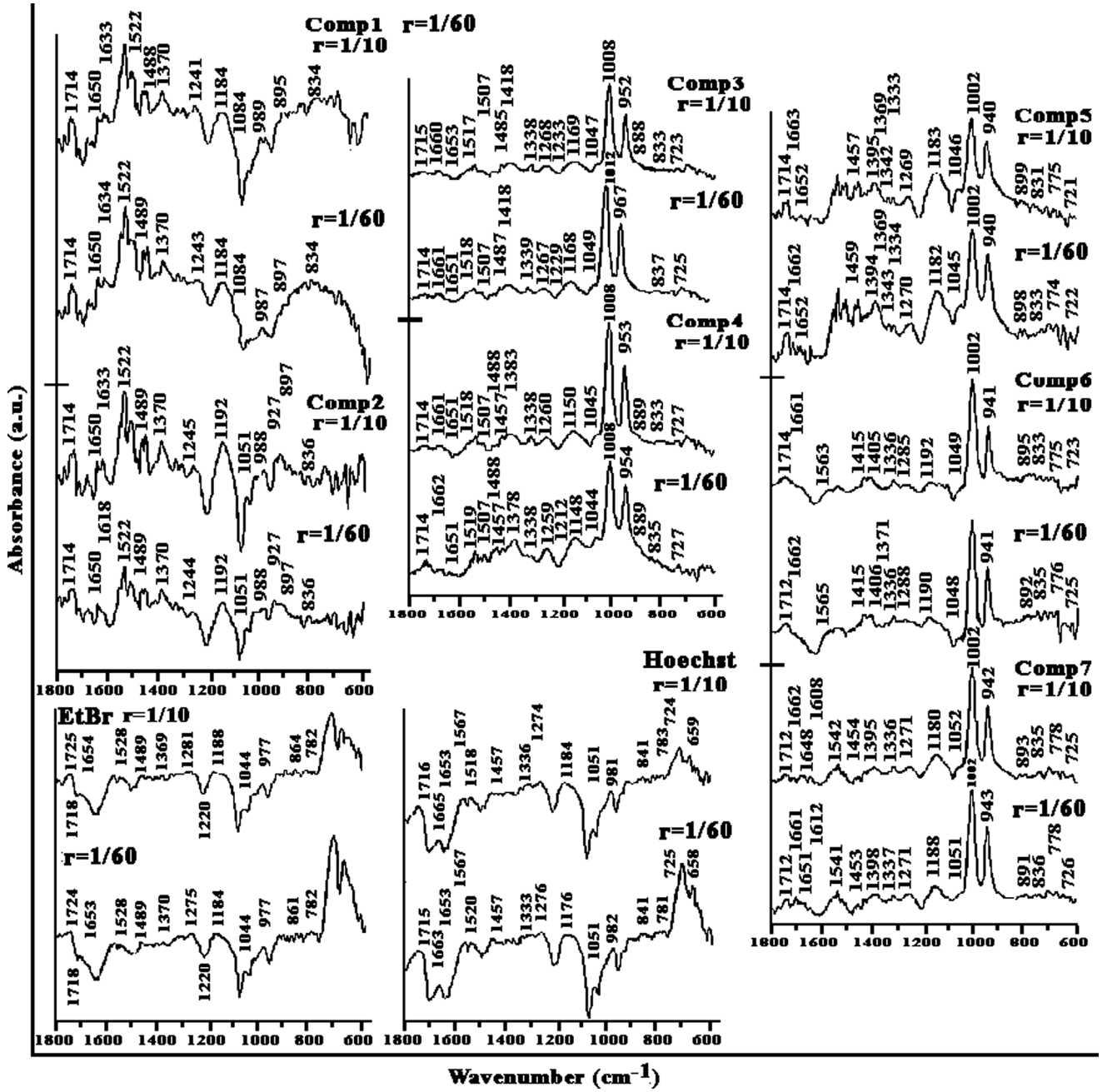

Fig. 8. Difference spectra of analog-DNA complexes in the region of 1800–600 $cm^{-1.}$

CT DNA shifted more for G and G-C peak in plane stretching vibration. Furthermore, the remarkable reduction has been observed in difference spectra of comp 3-DNA complex in intensity of guanine and cytosine absorption due to direct interaction of comp 3 with active sites of heterocyclic bases in the major and minor groove of DNA double helix [19,39]. However beta-carbolines with guanidine alkyl chain analogs, comp 5, 6 and 7 showed slight interaction at T and minor change in C and G-C peak.

Moreover, all the compounds have been observed to have major and minor interaction with phosphate group, phosphodiester bonds and DNA backbone. In difference spectra (Fig. 8), comp 3 showed positive shift around 1044 and 957 cm^{-1} as it has the less ability of external binding with phosphate sugar backbone of DNA double helix. Compared to ethidium bromide and Hoechst, peak shifting and intensity changes by comp 3 at 837 cm^{-1} attributed to base stacking interaction through major or minor groove binding. So, spectral changes observed for the sugar conformations, deoxyribose – phosphodiester chain vibrations and sugar-phosphate backbone stretching vibrations might be attributed to the slight external binding as groove binder. While, beta-carboline compounds with guanidine alkyl chain analogs have more affinity towards sugar moiety and have maximum ability to change the sugar conformation in DNA backbone. The explanation from these results ultimately showed that the reactive form of gamma carboline analog, comp 3, binds with DNA via G and transfer its free NH moiety to guanine and its small alkyl chain enters freely in the phosphate group as well as deoxyribose-phosphodiester bonds. This might be possible due to partial intercalation of comp 3 to CT DNA double helix making DNA unavailable for replication mechanism during cell division and ultimately stops its normal functioning.

3.1.4. Elucidation of mode of binding of the analogs with CT DNA

After analyzing the IR peaks to know the binding site and position of

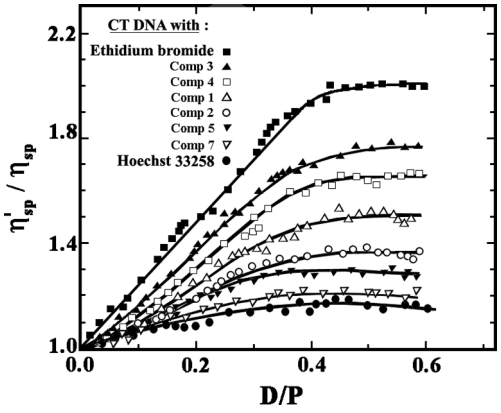

Fig. 9. Plot of change of relative specific viscosity of sonicated CT DNA (450 μM) with increasing concentration of comp1 (Δ-Δ), comp2 (○-○), comp3 (▲-▲), comp4 (□-□), comp5 (▼-▼), comp7 (∇-∇). The relative specific viscosities of the above compounds with CT DNA was compared with the change in specific viscosity of sonicated CT DNA with ethidium (■-■) and Hoechst 33,258 (●-●). The specific viscosity was calculated from Eq. (2) described in text.

the analog compounds at respective D/P ratios, the exact mode of binding of the synthetic compounds to the sonicated CT DNA has been further investigated by viscosity studies (Fig. 9). The changes of relative specific viscosity at respective D/P were compared with CT DNA-ethidium bromide and CT DNA- Hoechst 33,258 complexation as ethidium and hoechst 33,258 are known to be a classical intercalator and groove binder, respectively.

Among the analogs, change of relative specific viscosity against D/P has been found to be maximum for compound 3, which was very close to the curve of CT DNA-ethidium complex, followed by compound 4, compound 1, compound 2, compound 5, compound 6 (not shown in the figure) and compound 7. The changes were due to the fact that the axial length of the DNA enhances and it becomes more rigid after binding with the compounds. Hence, the viscosity increases as both the factors enhanced the frictional coefficient. Maximum change in relative specific viscosity was observed with compound 3-CT DNA, while changes were moderate with compound 4, compound 1 and compound 2, signifying an intercalative and partial interactive mode of binding. While, changes of relative specific viscosity with compound 5, 6, and 7, were very insignificant and close to Hoechst 33258- CT DNA curve, indicating groove or surface binding with sonicated CT DNA.

Based on the size, structure and functional group of the analog compounds, none of them showed complete intercalative mode of binding. Among all, only compound 3 and 4 showed partial intercalative binding while rest showed surface or groove binding involving hydrogen bond or electrostatic binding. Among the three sets, the series of analogs with amino alkyl chain, because of more localized charge density in the single amino group, showed maximum binding affinity with significant percent change of fluorescence intensity and remarkable stabilizing property to CT DNA. Furthermore, analog compounds with amino alkyl chain at delta position of the core molecule showed highest binding affinity with DNA followed by the compounds with amino alkyl chain at alpha position of the core molecule. In compounds with amino alkyl chain at delta position of the core molecule, the indole hydrogen is more freely available for participating in hydrogen bond with target molecule compared to the compounds with amino alkyl chain at alpha position of the core molecule, where the indole hydrogen because of steric hindrance of trifluoromethyl group, it is unable to participate in the bonding. While, the series of analogs with guanidine alkyl chain at the alpha position of the core molecule, because of the more stabilized and delocalization of the charge (positive charge in the guanidine shows some resonating structure with a switch over action among the two $-NH_2$ group present in the compound), showed comparatively lower binding and stabilizing properties with DNA. Furthermore, with all the above compounds, the trend of binding affinity with CT DNA decreases with increased chain length because of more bulky nature. Also, the bindings were entropically driven being more with guanidine alkyl chain analogs because of its more heavy chain length disrupting the surrounding water molecules of DNA. FTIR followed by viscosity analysis supported the partially intercalated state of binding of the compounds.

3.2. *In vitro* cytotoxicity and anti proliferative effect of analog compounds

The ultimate objective of these synthetic analogs is to highlight their therapeutic role by emphasizing the anti proliferative effect by apoptotic induction ability of the compounds in different cancer cell lines. Hence binding study follows *in vitro* cytotoxicity. Apoptosis is a carefully regulated programmed death, energy dependent process, by which cells are physiologically eliminated in metazoan organisms. Inhibition of cell proliferation by increasing apoptosis in tumor cells is the effective ways to control the tumor growth and cancers. During apoptotic death, cells are neatly carved up by caspases and packaged into apoptotic bodies as a mechanism to avoid immune activation [50–56]. However two more non-apoptotic deaths processes are also reported necrotic and autophagic death. Necrosis have a biological function where an immune reaction to the dying cell is desirable such as in microbial infection, while in certain populations of apoptosis-resistant cells such as neurons or brain cells, autophagy can be observed following growth factor withdrawal, where nutrient uptake declines [50–56]. Hence, apoptosis is considered as one of the trademark of the anti cancer drug. It is triggered by various stimuli and characterized by a series of distinct biochemical and morphological changes [50–56]. This section of the study mainly focused on the *in vitro* anti-proliferative effect of the analog compounds in HeLa (cervical carcinoma), MDA-MB-231 (breast carcinoma), A549 (lung carcinoma), A375 (skin carcinoma), ACHN (kidney carcinoma), HCT116 (colon cancer cell line) and $HepG_2$ (liver epitheloid carcinoma) cancer cell lines thereby inducing apoptosis. These cell lines represented the most prevalent type of cancer worldwide. Additionally, HCT 116, HepG2 and MDA-MB-231 are the most resistant cells to the conventional therapies [57–59].

MTT assay was followed to evaluate the cytotoxic activity of the analog compounds 1–7 on the above mentioned cancer cell lines. After

Table 3
MTT assay with GI_{50} values in μM[a] on different cancer cell lines after 24 hrs of treatment.

Carboline compounds	HCT 116	HepG2	A375	MDA MB 231	HeLa	A549	ACHN
Comp 1	20.9 ± 1.6	31.6 ± 2.0	65.5 ± 3.0	83.3 ± 2.5	72.8 ± 2.5	62 ± 2.5	66.2 ± 1.9
Comp 2	22 ± 1.8	33 ± 2.5	72 ± 3.0	85.6 ± 3.0	93.4 ± 3.0	113.6 ± 3.5	68 ± 3.0
Comp 3	6.2 ± 1.2	8.3 ± 1.0	15.4 ± 1.5	24 ± 1.5	31.2 ± 1.5	39 ± 1.5	40.1 ± 1.9
Comp 4	8.9 ± 1.2	9.1 ± 1.2	22.3 ± 2.0	40.3 ± 1.8	41 ± 1.8	41.8 ± 1.8	48 ± 1.9
Comp 5	18.5 ± 1.6	27 ± 1.9	59.5 ± 2.5	78 ± 2.5	65.7 ± 2.5	59.5 ± 2.0	57.6 ± 2.0
Comp 6	12.6 ± 1.5	25.8 ± 1.6	45.5 ± 2.5	46.8 ± 2.1	50.8 ± 2.1	55 ± 1.9	56.8 ± 2.7
Comp 7	11.8 ± 1.3	22.7 ± 1.5	25.2 ± 2.0	41.6 ± 2.1	42.5 ± 2.1	43.1 ± 1.8	52.1 ± 2.5

[a] Average of three individual experiments at same conditions.

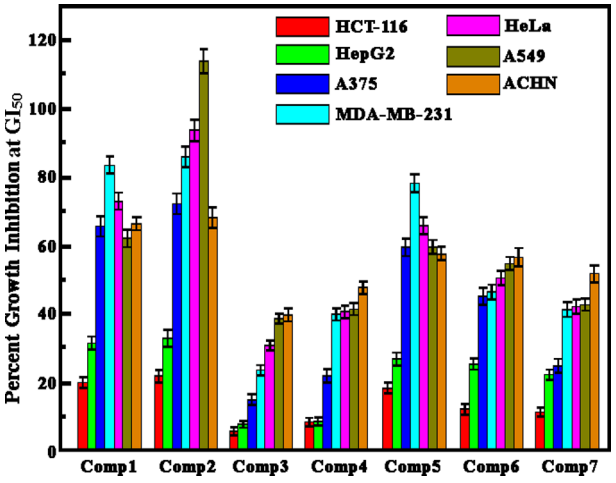

Fig. 10. Percentage growth inhibition of HeLa (cervical carcinoma), MDA-MB-231 (breast carcinoma), A549 (lung carcinoma), A375 (skin carcinoma), ACHN (kidney carcinoma), HCT116 (colon cancer cell line), $HepG_2$ (liver epitheloid carcinoma), HEK and WRL-68 cells following treatment with the analog compounds (1–7) of varying concentrations as described in the text for 24 h of incubation. Data are statistically analyzed with ANOVA test and significant values are calculated against both untreated as well as solvent control ($^{*}P < 0.05$ vs. solvent control).

24 h treatment with the compounds, it was found that the above cell lines showed different GI_{50} values depending on the concentrations of the compounds (Table 3, Fig. 10). Out of the three parameters, 50% maximum growth inhibitory dose of the compound was considered to be the effective dose to measure its cytotoxicity. Compound 1 showed GI_{50} values of 72.8 ± 2.5 μM in HeLa cells, 83.3 ± 2.5 μM in MDA-MB-231, 62.0 ± 2.5 μM in A549, 65.5 ± 3.0 μM in A375, 66.2 ± 1.9 μM in ACHN, 20.9 ± 1.6 μM in HCT-116 and 31.6 ± 2.0 μM in $HepG_2$, respectively. Similarly, compound 2, showed

Table 4
Comparison between % Apoptosis and Necrosis through Annexin V-FITC/PI assay.[a]

Added concentrations of comp 3	$FITC^+/PI^-$ (apoptotic cell%)	$FITC^+/PI^+$ (Necrotic cell%)
0 (Control)	5.67	0.51
3 μM (GI_{25})	22.06	10.14
6.2 μM (GI_{50})	36.73	17.80
9 μM (GI_{75})	40.02	43.66

[a] Average of three individual experiments at same conditions.

GI_{50} values of 93.4 ± 3.0 μM in HeLa cells, 85.6 ± 3.0 μM in MDA-MB-231, 113.6 ± 3.5 μM in A549, 72.0 ± 3.0 μM in A375, 68.0 ± 3.0 μM in ACHN, 22.0 ± 1.8 μM in HCT116 and 33.0 ± 2.5 μM in $HepG_2$. Compound 3 was analyzed to show GI_{50} values of 31.2 ± 1.5 μM in HeLa cells, 24 ± 1.5 μM in MDA-MB-231, 39.0 ± 1.5 μM in A549, 15.4 ± 1.5 μM in A375, 40.1 ± 1.9 μM in ACHN, 6.2 ± 1.5 μM in HCT-116 and 8.3 ± 1.0 μM in $HepG_2$. Compound 4 gave GI_{50} values of 41.0 ± 1.8 μM in HeLa cells, 40.3 ± 1.8 μM in MDA-MB-231, 41.8 ± 1.8 μM in A549, 22.3 ± 2.0 μM in A375, 48.0 ± 1.9 μM in ACHN, 8.9 ± 1.2 μM in HCT116 and 9.1 ± 1.2 μM in $HepG_2$. Compound 5 showed GI_{50} values of 65.7 ± 2.5 μM in HeLa cells, 78 ± 2.5 μM in MDA-MB-231, 59.5 ± 2.0 μM in A549, 59.5 ± 2.5 μM in A375, 57.6 ± 2.0 μM in ACHN, 18.5 ± 1.6 μM in HCT116 and 27.0 ± 1.9 μM in $HepG_2$. Compound 6 gave GI_{50} values of 50.8 ± 2.1 μM in HeLa cells, 46.8 ± 2.1 μM in MDA-MB-231, 55.0 ± 1.9 μM in A549, 45.5 ± 2.5 μM in A375, 56.8 ± 2.7 μM in ACHN, 12.6 ± 1.5 μM in HCT116 and 25.8 ± 1.6 μM in $HepG_2$ and compound 7 was tested for GI_{50} values of 42.5 ± 2.1 μM in HeLa cells, 41.6 ± 2.1 μM in MDA-MB-231, 43.1 ± 1.8 μM in A549, 25.2 ± 2.0 μM in A375, 52.1 ± 2.5 μM in ACHN, 11.8 ± 1.3 μM in HCT116 and 22.7 ± 1.5 μM in $HepG_2$. Hence, the smallest alkyl chain analog attached to gamma position, Compound 3, showed maximum cytotoxicity

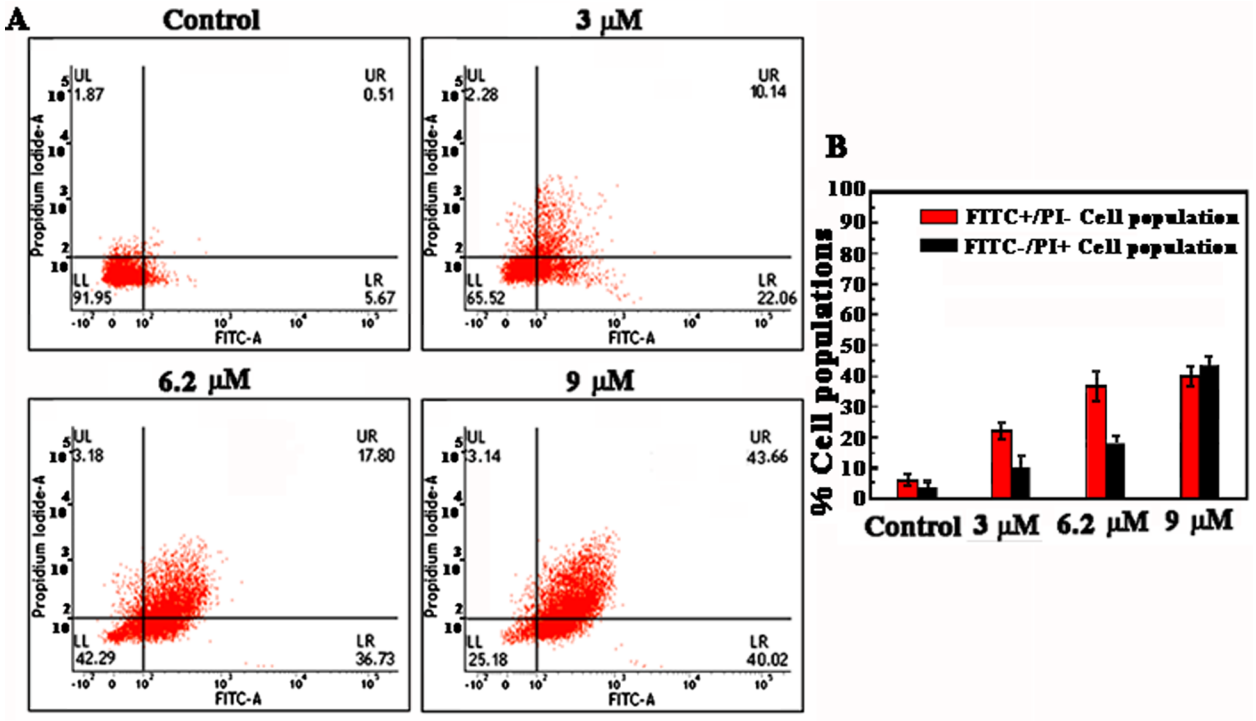

Fig. 11. (A) Contour diagram of FITC-Annexin V/PI flow cytometry of HCT116 cells after 12 h of incubation at untreated, GI_{25}, GI_{50} and GI_{75} concentrations of 0, 3.0, 6.2 and 9.0 μM respectively. Data are representative of three independent experiments. (B) Bar graph presentation of quantitative results of comparison between apoptotic and necrotic population of HCT-116 cells after treatment with compound 3 (Table 4).

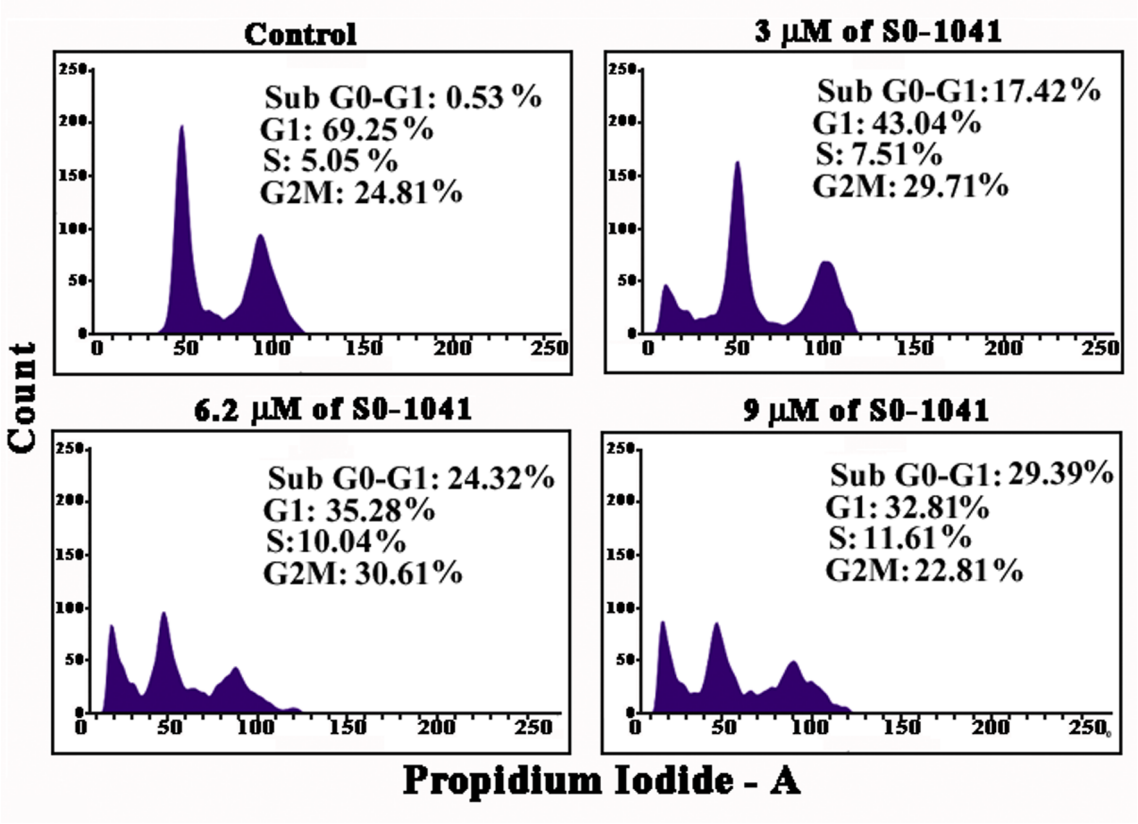

Fig. 12. Cell cycle analysis of comp3 treated HCT116 cells at 3.0 µM, 6.2 µM and 9.0 µM for 12 h of incubation. Data are representative of three independent experiments, and the means are significant compared with their control ($P < 0.05$) (Table 5).

Table 5
Cell cycle analyses[a] of Comp 3-treated HCT 116 cells analyzed by using PI staining.

Added concentrations of comp 3	Sub-G0-G1	G0/G1	S	G2/M
Control	0.53 ± 0.01%	69.25 ± 0.20%	5.05 ± 0.12%	24.81 ± 0.19%
GI25 (3 µM)	17.42 ± 0.07%	43.04 ± 0.18%	7.51 ± 0.14%	29.71 ± 0.21%
GI50 (6.2 µM)	24.32 ± 0.12%	35.28 ± 0.16%	10.04 ± 0.13%	30.61 ± 0.26%
GI75 (6.2 µM)	29.39 ± 0.16%	32.81 ± 0.17%	11.61 ± 0.11%	22.81 ± 0.31%

[a] Average of three individual experiments at same conditions.

with GI_{50} value of 6.2 uM against HCT-116, followed by comp4 > comp7 > comp6 > comp5 > comp2 and > comp1 (Table 3). However, for HEK and WRL-68, the normal epithelial cell lines, it was followed up to concentration of 65 µM each, for measuring its GI_{50} values, beyond this concentration the Beer-Lambert's law was not obeyed by the compounds hence could not proceed. Therefore it can be predicted that HEK-293 and WRL-68 might have GI_{50} values more than 65 µM.

Earlier also beta carboline alkaloids and its various derivatives have been reported to show *in vitro* cytotoxicity in many cancer cell lines [58–63]. But it was never correlated to their binding affinity with the target specific macromolecules. Furthermore, the author had also reported the GI_{50} values in natural beta-carboline alkaloids like harmalol and harmaline, where not only that the values were reported to be much higher than the GI_{50} values obtained with these synthetic compounds but also the incubation time was about 48 h, 24 h more than with the analogs [18,33].

Since, the highest degree of concentration dependent increase in growth inhibition was observed in the HCT-116 colon cancer cell line with compound 3, henceforth, other parameters in support of apoptosis were analyzed only in the HCT-116 cell line to further study the efficacy of compound 3 in detail.

3.3. Apoptotic induction ability of comp3 on HCT-116 cell line

Treatment with compound 3, induced phosphatidylserine (PS) externalization in HCT-116 cells, which is again another remarkable characteristic of early stage of apoptosis. Fig. 11A showed the quantitative results of bivariate FITC-Annexin V/PI FCM of HCT-116 cells after treatment with the compound for different concentrations (at GI_{25}, GI_{50} and GI_{75} concentrations of 3, 6.2 and 9.0 µM respectively). The lower left quadrant of the cytograms showed the viable cells (control cells), which excluded PI and are negative for FITC-Annexin V binding because of intact cytoplasmic membrane. The upper right quadrant represented the non-viable, necrotic cells, positive for FITC-Annexin V binding, showing PI uptake. Furthermore, the lower right quadrant represented the apoptotic cells, which was FITC-Annexin V positive and PI negative, demonstrating Annexin V binding to PS with cytoplasmic membrane integrity. The $FITC^+/PI^-$ apoptotic cell population increased gradually from 5.67 ± 0.5% in control to 22.06 ± 1.3% after treatment with 3 µM, 36.73 ± 1.6% after treatment with 6.2 µM and 40.02 ± 2.1% after treatment with 9.5 µM of compound 3, respectively. On the other hand FITC+/ PI + necrotic cell population was increased from 0.51 ± 0.4% to 43.66 ± 1.4% after 24 h of treatment with the compound. Fig. 11B represents the bar graph presentation of

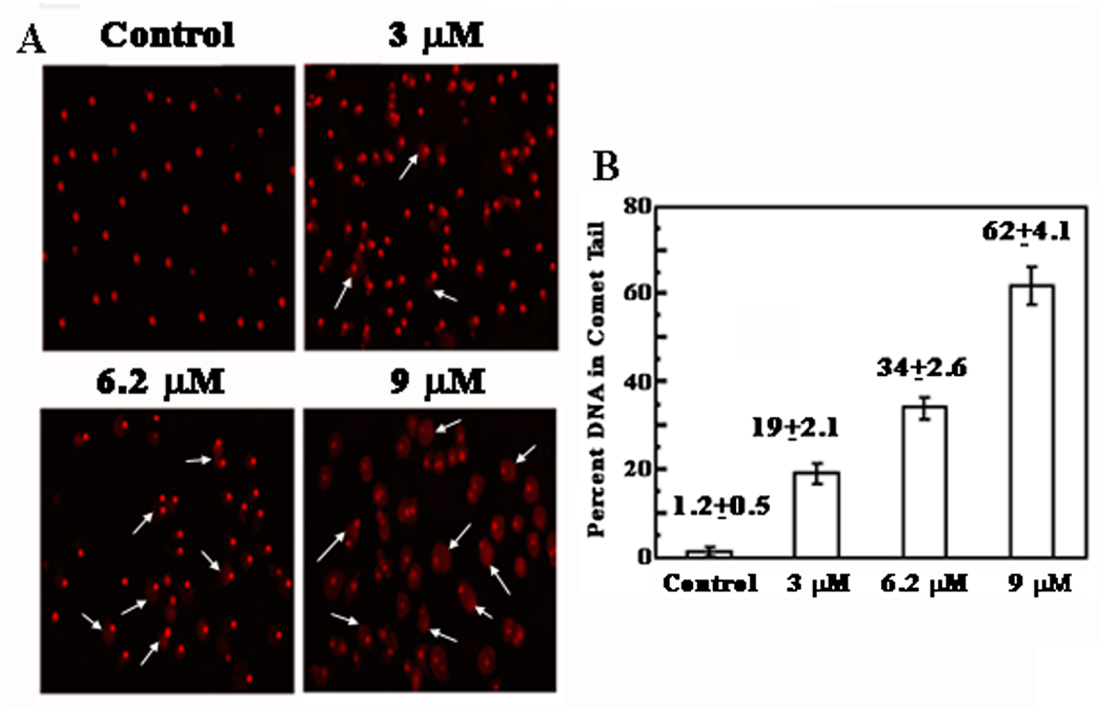

Fig. 13. (A) Single cell gel electrophoresis showing detectable comet tails (marked with arrows) with increasing concentration of comp3, indicative of DNA damage. (B) Bar graph representation of effect of comp3 treatment on % DNA of HCT-116 cell in the comet tail using the software Casp (Table 6). The graph displays the mean ± SD (standard deviation) of three independent experiments.

Table 6
CASP software analysis for the calculation of % DNA[a] in comet tail appeared due to DNA fragmentation by adding comp 3 treated HCT 116 cancer cells.

Added concentrations of comp 3	% DNA in comet tail	± S.D
0 (Control)	1.2	0.5
3 μM (GI_{25})	19	2.1
6.2 μM (GI_{50})	34	2.6
9 μM (GI_{75})	62	4.1

[a] Average of three individual experiments at same conditions.

quantitative results of comparison between apoptotic and necrotic population of HCT-116 cells (Table 4.) after treatment with compound 3 to determine dose of choice.

Cell cycle analyses of compound 3-treated HCT-116 cells were further analyzed by using PI staining, and the cell distributions were expressed for sub-G0/G1, G0/G1, S and G2/M phases (Fig. 12 and Table 5.). Dose kinetics study of compound 3-treated cells indicated increasing accumulation of cells at sub-G0/G1 phase. The percentage of sub-G0/G1 arrest was increased from 0.53 ± 0.01 to 17.42 ± 0.07, 24.32 ± 0.12 and 29.39 ± 0.16% after the treatment of 3, 6.2 and 9 μM of compound 3 for 24 h incubation in HCT-116 cells, respectively (Fig. 12). Through remarkable increase in sub-G0/G1 population in cell cycle arrest, we can assume the high killing power preferably antiproliferative action of compound 3 [66,67]. In this sub-G0/G1 population few cells are arrested via apoptosis and few cells are killed by necrosis. Generally at higher dose, necrosis is found to be maximum than apoptosis though the cell populations increases simultaneously. So the choice of concentration for the drug should be below GI_{75}. By addition of 6.2 μM of compound 3 at GI_{50}, with the gradual increase in percentage of sub-G0/G1 arrest, G2/M percentage also increases from 24.81 ± 0.19 to 29.71 ± 0.21 and 30.61 ± 0.26% at control, GI_{25} and GI_{50} respectively, while at GI_{75} it decreased to 22.81 ± 0.31%, emphasizing the ultimate cell cycle arrest at G2/M phase [64,65].

DNA fragmentation from the activation of endonucleases, is one of the later steps in apoptosis [66–68]. Hence, we further characterized the apoptotic HCT-116 cells by single cell gel electrophoresis or comet tail assay (Fig. 13). The results showed more DNA strand breaks (Table 6) constituting of 62 ± 4.1% DNA (longest tail length) with the treatment of compound 3 at 9 μM of concentration and least amount of DNA (19 ± 2.1%) with lowest concentration of 3 μM (Fig. 14A), while at GI_{50} of 6.2 μM, 34 ± 2.6% DNA was observed in comet tail as calculated using the software Casp. The result was further presented graphically (Fig. 13B)

Phase contrast microscopic, scanning electron microscopic (SEM) and transmission electron microscopic (TEM) images were used to further characterize the size, surface contour and ultramorphology of the drug (compound 3) treated HCT-116 cells. The Phase contrast microscopic images showed more number of round shaped dead cells (marked with white arrows) with increasing concentration of the compound (Fig. 14A). The morphology of the treated and untreated cells as observed by SEM, was shown in Fig. 14B. The morphological changes observed were cytoplasmic blebbing, shrinkage as well as irregularities in cell contour and size in the drug treated conditions. Whereas, untreated controlled HCT-116 cell line retain the organotypic spheroids as small scale brush structures and remain spread out without any sign of irregularities in cell contour and size. Furthermore, ultramorphological study by TEM, which is used to examine the structure and composition of thin sections of the tissue in submicron detail, was performed by TECNAI 200KV TEM from All India Institute of Medical Sciences, India (Fig. 14C). The image of controlled section of colonic epithelial cells with deep invaginations into the cell wall called crypts have been observed and these crypts gradually lost in treated conditions. Control HCT-116 contains many lipid droplets, which reduces in number in dose dependent manner. In apoptotic HCT-116 cell, the ratio of area of nucleolus vs. cytoplasm becomes double but the size of nucleus gets reduced with more condensed structure. Further, the number of mitochondria reduces with increasing number of vacuoles in apoptotic cells highlighting the therapeutic role of compound 3 on HCT-116. Immuno fluorescence with anti active caspase 3 and p53 (Fig. 15) was performed to see the analysis of the apoptotic biomarkers at the protein level. Simultaneously nuclear accumulation by DAPI of excess

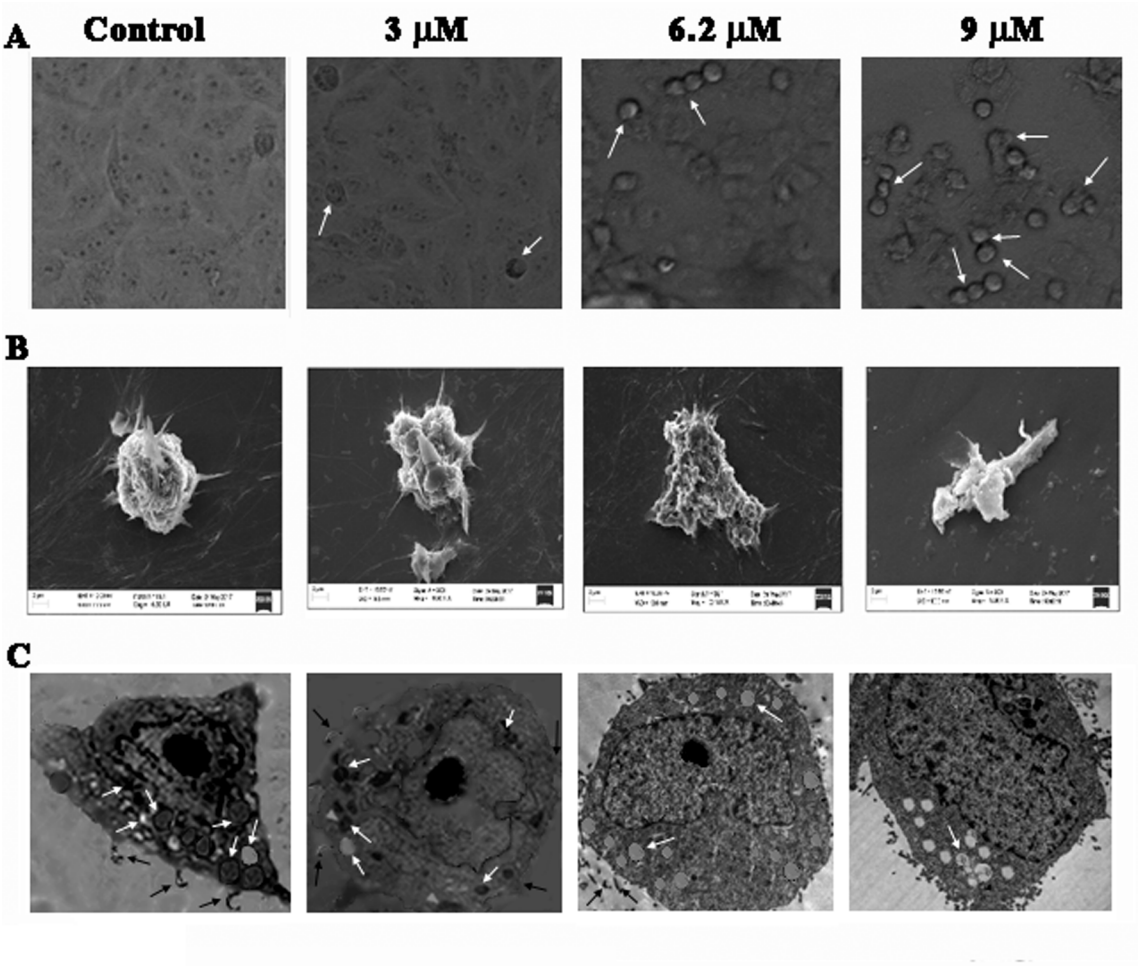

Fig. 14. (A) Morphology of control cells and comp3 (of increasing concentration) treated cells for 12 h observed under confocal microscope (10× magnifications). (B) Changes in cell morphology and apoptotic index parameters as observed using S530 Hitachi scanning electron microscope (SEM) and (C) Transmission electron micrograph (TEM) of untreated HCT116 cells showing large number of cell crypts and lipid droplets formation. With the treatment of comp3, nucleus gets reduced with more condensed structure, number of mitochondria get reduced with increasing number of vacuoles formation. All the positive changes are marked with arrows.

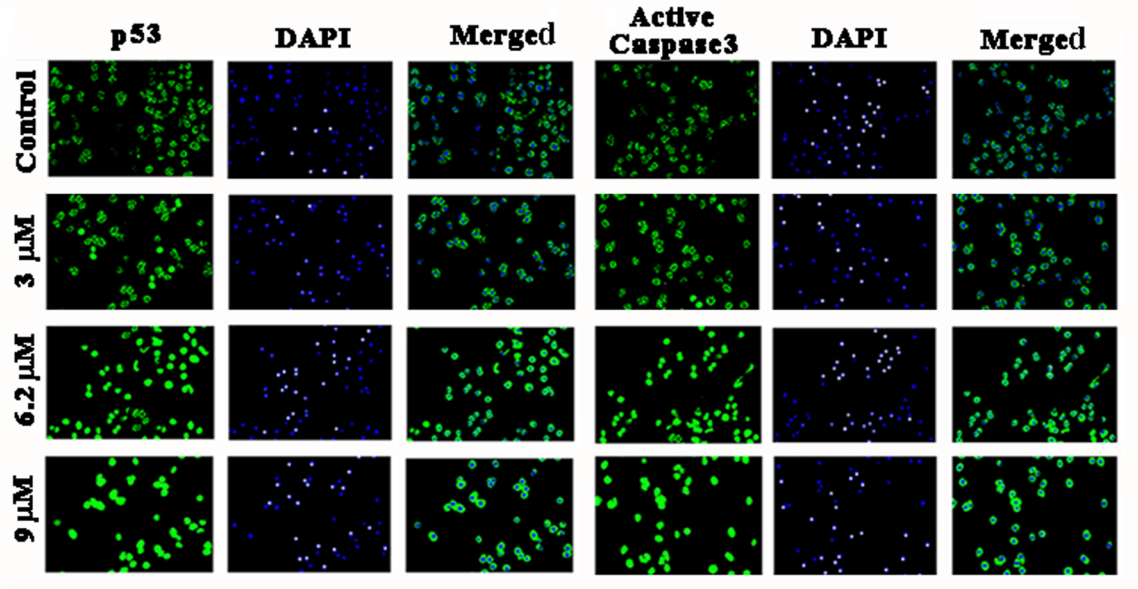

Fig. 15. Immunocytochemical localization of active caspase 3 and p53 in HCT116 cells by confocal microscope after exposure to 3.0, 6.2 and 9.0 μM of comp3 for 12 h.

concentration of active casepase 3 and p53 of apoptotic HCT-116 cell was shown. The expression of p53 and caspase-3 that favored apoptosis, were up-regulated in a dose dependent manner. Evidences suggested that it is through mitochondrial cytochrome c release that p53 induces apoptosis by caspase activation. Principally, p53 tumor suppressor gene is involved in the regulation of cell cycle, DNA repair, and apoptosis, leading to caspase activation [68–70].

With the intension to change the preferred conformation of the piperidine ring due to the higher conformational energy as compared to an alkyl group (2.1 and 1.8 kcal/mol respectively) CF_3-group in the core molecule of tetrahydro-carboline has been incorporated with amino alkyl chain at alpha position (compound 1 and 2), amino alkyl chain at delta position (compound 3 and 4) and guanidine alkyl chain at alpha position (compound 5, 6 and 7), respectively. They were synthesized by Pictet-Spengler cyclization starting from tryptamine or isotrypatamine and cyclic trifluoromethylated imines. It is very important as with this incorporation, there is the possibility to modulate basicity and nucleophilicity of the nitrogen atom at the 2-position to avoid the use of protective groups.

However, considering DNA as the sole target molecule in cancer therapy, the ability of the above analog compounds to target nucleic acid structure and function, detail studies were performed to exploit those small molecules as futuristic therapeutic agents against cancer. In this case, binding and the apoptotic induction ability of seven novel synthetic compounds *viz.* 1 and 2 with amino alkyl chain at the alpha position of the tetrahydro carboline core molecule, 3 and 4 with amino alkyl chain at the delta position of the core molecule and 5, 6 and 7 with guanidine alkyl chain at the alpha position of the core molecule, respectively, in seven cancer cell lines *viz.* HeLa, MDA-MB-231, A549, A375, ACHN, HCT116, $HepG_2$ have been reported. The outcomes significantly helped in screening the best binding analog compound along with anticancer activity following evidence of antineoplastic properties.

Regarding cytotoxic and growth inhibition ability of the analogs on cancer cell lines, all the analogs found to be very potent against HCT116 (colon carcinoma) followed by HepG2 (liver carcinoma), restricting the cell cycle at G2/M phase. The smallest alkyl chain analog at the delta position of the core molecule i.e. compound 3, showed maximum cytotoxicity with GI_{50} value of 6.2 uM against HCT-116, followed by the guanidine alkyl chain compounds. The maximum cytotoxic and anti neoplastic ability of compound 3 is probably because of its maximum binding affinity with target specific DNA macromolecules and its small light chain analog, while as the chain length increases the binding affinity along with the cytotoxic potency of higher amino alkyl chain compounds decreases. Previously also gamma-carboline derivative compounds have been reported to be more potent synthetic drug than beta-carboline compounds [23–25]. However with the guanidine alkyl chain compounds, unlike their trend of binding affinity to DNA, cytotoxicity is more as the guanidine alkyl chain length increases. This trend of guanidine headed alkyl chain compound was also reported by others [71–74]. Guanidine headed group with an extension of alkyl chain between the backbone and the head is superior to other cationic subunits and provides superior transporter, since this is apparently a critical structural determinant of cellular uptake and hence more cytotoxic potency [71–74]. Guanidinium rich scaffolds facilitate cellular translocation and delivery of bioactive cargos through biological barriers. Charge pairing and hydrogen bonding with cell surface counterparts have been proposed, though their exact role is assumed. The Y-shaped guanidinium group is a highly symmetric planar functionality that can form two strong parallel hydrogen bonds with biologically relevant counterparts. Its geometry generates a more favorable hydrogen bond alignment compared to ammonium group which are also widely found in biomolecules. Additionally binding can occur through both charge pairing and hydrogen bonding as the group maintains its protonated state over a wide range of pH (pK_a 13.5). Moreover, unlike for the ammonium cations where the charge is localized, the interaction with ions like phosphates is facilitated by delocalization of positive charge in guanidinium group [71–74]. Thus in spite of being a poor DNA target molecule, the compounds with guanidine moiety attached to alkyl chain showed superior cytotoxicity and probably because of more preference in terms of binding towards any surface transport receptor or any other macromolecule other than DNA. However the actual pathway for their entry into cells has remained controversial and the fundamental understanding of the entry process is still lacking and demands further research.

4. Conclusions

In summary, the study contributes new information on specific molecular target by the small molecules based on structure-activity relation that ultimately open up new insights for drug designing in future. Screening through binding and *in vitro* cytotoxic assays, compound 3 from series of gamma carboline with the shortest amino alkyl chain, found to be the most potent cytotoxic compound against colon cancer cell line HCT-116, targeting DNA. Probably, partial intercalation of comp3 prevents information retrieval from DNA, leading to the arrest of cell division including abnormal cell proliferation in cancer.

However, in spite of weak DNA affinity, efficacy of the beta carboline with guanidine alkyl chain compounds (compound 5, 6 and 7) cannot be neglected that probably target other surface specific receptor molecule. The molecular mechanism of action and activation of the compounds need further in depth study.

Acknowledgements

Authors are grateful to DST-RFBR 2017-19 (DST/INT/RUS/RFBR/P-254), India and RFBR 17-53-45068, Russia for funding. SS, Research Associate, is supported by grants from DST, NPDF, India. Authors are also grateful to DST-PURSE, DST-FIST (SR/FST/LSI-467/2010C) & PRG, University of Kalyani, 2017–18 for their partial financial support.

Conflict of interests

No competing financial interests exist. The authors declare no conflict of interest.

Appendix A. Supplementary material

Supplementary data to this article can be found online at https://doi.org/10.1016/j.bioorg.2019.01.028.

References

[1] M.J. Waring, DNA modification and cancer, Ann. Rev. Biochem. 50 (1) (1981) 159–192.
[2] L.H. Hurley, DNA and its associated processes as targets for cancer therapy, Nat. Rev. 2 (3) (2002) 188–200.
[3] S.C. Prasad, I. Roy, Nucleic acid based therapeutic molecules, CRIPS 9 (3) (2008) 49–55.
[4] M.F. Roberts, M. Wink, Biochemistry, in: M.F. Roberts, M. Wink (Eds.), Ecology and Medicinal Applications, Alkaloids, vol. 1, Plenum Press, New York, London, 1998.
[5] K. Bhadra, G.S. Kumar, Therapeutic potential of isoquinoline alkaloids: An update on their nucleic acids binding aspects and implications for drug design, Med. Res. Rev. 31 (6) (2011) 821–862.
[6] R. Ali, Z. Mirza, G.M. Ashraf, M.A. Kamal, S.A. Ansari, G.A. Damanhouri, A.M. Abuzenadah, A.G. Chaudhary, I.A. Sheikh, New anticancer agents: recent developments in tumor therapy, Anticancer Res. 32 (7) (2012) 2999–3005.
[7] M. Moudi, R. Go, C.Y. Yien, M. Nazre, Vinca alkaloids, Int. J. Prev. Med. 4 (11) (2013) 1231–1235.
[8] G.S. Kumar, G. Brahmachari (Eds.), Chemistry and Biology, Wiley-VCH Verlag GmbH & Co. KGaA, 2015.
[9] D.H. Aarons, G.V. Rossi, R.F. Orzechowski, Cardiovascular actions of three harmala alkaloids: harmine, harmaline and harmalol, J. Pharm. Sci. 66 (9) (1997) 1244–1248.
[10] A.F.M. Abdel Fattah, K. Matsumoto, Y. Murakami, K.A.W. El-Hady, M.F. Mohamed, H. Watanabe, Inhibitory effect of harmaline on the tryptophan induced 5-hydroxy syndrome and body temperature changes in pargyline-pretreated rats, Jpn. J. Pharmacol. 72 (1) (1996) 39–47.

[11] M. Mahmoudian, H. Jalilpour, P. Salehian, Toxicity of *Peganum harmala*: Review and a case report, Iran. J. Pharmacol. Ther. 1 (1) (2002) 1–4.
[12] R. Cao, W. Peng, Z. Wang, A. Xu, β-carboline alkaloids: biochemical and pharmacological functions, Cur. Med. Chem. 14 (4) (2007) 479–500.
[13] T.J. Herraiz, Identification and occurrence of beta-carboline alkaloids in raisins and inhibition of monoamine oxidase (MAO), Agric. Food Chem. 55 (21) (2007) 8534–8540.
[14] K. Patel, M. Gadewar, R. Tripathi, S.K. Prasad, D.K. Patel, A review on medicinal importance, pharmacological activity and bioanalytical aspects of β-carboline alkaloid "Harmine", Asian Pac. J. Trop. Biomed. 2 (8) (2012) 660–664.
[15] S. Sarkar, K. Bhadra, Binding of alkaloid harmalol to DNA: photophysical and calorimetric approach, J. Photochem. Photobiol. B Biol. 130 (2014) 272–280.
[16] S. Sarkar, P. Pandya, K. Bhadra, Sequence specific binding of beta -carboline alkaloid harmalol with deoxyribonucleotides: binding heterogeneity, conformational, thermodynamic and cytotoxic aspects, PLoS ONE 9 (9) (2014) 1–14.
[17] P. Bhattacharjee, S. Sarkar, P. Pandya, K. Bhadra, Targeting different RNA motifs by beta carboline alkaloid, harmalol: a comparative photophysical, calorimetric and molecular docking approach, J. Biomol. Struct. Dyn. 34 (12) (2015) 2722–2740.
[18] P. Bhattacharjee, T. Ghosh, S. Sarkar, P. Pandya, K. Bhadra, Binding affinity and *in vitro* cytotoxicity of harmaline targeting different motifs of nucleic acids: an ultimate drug designing approach, J. Mol. Recog. 31 (4) (2017) 1–16.
[19] S. Nafisi, M. Bonsaii, P. Maali, M.A. Khalilzadeh, F. Manouchehri, β-carboline alkaloids bind DNA, J. Photochem. Photobiol. B Biol. 100 (2) (2010) 84–91.
[20] R. Cao, Q. Chen, X. Hou, H. Chen, H. Guan, Y. Ma, W. Peng, A. Xu, Synthesis, acute toxicities, and antitumor effects of novel 9-substituted beta-carboline derivatives, Bioorg. Med. Chem. 12 (17) (2004) 4613–4623.
[21] H. Guan, H. Chen, W. Peng, Y. Ma, R. Cao, X. Liu, A. Xu, Design of beta-carboline derivatives as DNA-targeting antitumor agents, Eur. J. Med. Chem. 41 (10) (2006) 1167–1179.
[22] S.S. Kumar, M. Mariappan, Synthesis and *in vitro* cytotoxic activity of some novel β-carbolines bearing pyrrol-2-one moity, Int. J. Pharma Sci. Res. 4 (3) (2013) 47–53.
[23] P. Fosse, B. Rene, J.M. Saucier, C.H. Nguyen, E. Bisagni, C. Paoletti, Stimulation by gamma-carboline derivatives (simplified analogues of antitumor ellipticines) of site specific DNA cleavage by calf DNA topoisomerase II, Biochem. Pharmacol. 39 (4) (1990) 669–676.
[24] E.E. Kiseleva, A.S. Zakharevskiĭ, I.N. Nikiforova, The anti-allergic activity and mechanism of action of gamma-carboline derivatives, Farmakol. Toksikol. 53 (11) (1990) 22–24.
[25] R. Otto, R. Penzis, F. Gaube, T. Winckler, D. Appenroth, C. Fleck, C. Trankle, J. Lehmann, C. Enzensperger, Beta and gamma carboline derivatives as potential anti-Alzheimer agents: a comparison, Eur. J. Med. Chem. 87 (24) (2014) 63–70.
[26] V.M. Muzalevskiy, V.G. Nenajdenko, A.V. Shastin, E.S. Balenkova, G. Haufe, α-Trifluoromethyl-β-aryl enamines in the synthesis of trifluoromethylated heterocycles by the Fischer and the Pictet-Spengler reactions, Tetrahedron 65 (2009) 7553–7561.
[27] O.I. Shmatova, V.N. Khrustalev, V.G. Nenajdenko, From cyclic CF3-ketimines to a family of trifluoromethylated nazlinine and trypargine analogues, Org. Let. 18 (18) (2016) 4494–4497.
[28] L.M.M. Cesar-Tognoli, S.D. Salamoni, A.A. Tavares, C.F. Elias, J.C. Da Costa, J.C. Bittencourt, M.S. Palma, Effects of Spider Venom Toxin PWTX-I (6-Hydroxytrypargine) on the central nervous system of rats, Toxins 3 (2) (2011) 142–162.
[29] M.A. Kabeshov, B. Musio, P.R.D. Murray, D.L. Browne, S.V. Ley, Expedient preparation of nazlinine and a small library of indole alkaloids using flow electrochemistry as an enabling technology, Org. Lett. 16 (17) (2014) 4618–4621.
[30] I. Ojima, J.R. McCarthy, J.T. Welch (Eds.), Biomedical Frontiers of Fluorine Chemistry; ACS Symposium Series 639, American Chemical Society, Washington, 1996.
[31] J.P. Beeguee, D. Bonnet-Delpon, Bioorganic and Medicinal Chemistry of Fluorine, John Wiley & Sons, Hoboken, 2008, pp. 1–384.
[32] S. Chatterjee, S. Mallick, F. Buzzetti, G. Fiorillo, T.M. Syeda, P. Lombardi, K. Das Saha, G.S. Kumar, New 13-pyridinealkyl berberine analoguesintercalate to DNA and induce apoptosis in $HepG_2$ and MCF-7 cells through ROS mediated p53 dependent pathway: biophysical, biochemical and molecular modeling studies, RSC Adv. 5 (110) (2015) 90632–90644.
[33] S. Sarkar, P. Bhattacharjee, K. Bhadra, DNA binding and apoptotic induction ability of harmalol in $HepG_2$: biophysical and biochemical approaches, Chem. Biol. Interact. 258 (2016) 142–152.
[34] C.A. Parker, W.T. Rees, Correction of fluorescence spectra and measurement of fluorescence quantum efficiency, Analyst 85 (1013) (1960) 587–600.
[35] R. Sinha, M.M. Islam, K. Bhadra, G.S. Kumar, A. Banerjee, M. Maiti, The binding of DNA intercalating and groove binding compounds to A-form and protonated form of poly(rC).poly(rG): spectroscopic and viscometric study, Bioorg. Med. Chem. 14 (3) (2006) 800–814.
[36] K. Bhadra, M. Maiti, G.S. Kumar, Molecular recognition of DNA by small molecules: AT base pair specific intercalative binding of cytotoxic plant alkaloid palmatine, BBA 1770 (7) (2007) 1071–1080.
[37] S. Alex, P. Dupuis, FTIR and Raman investigation of cadmium binding by DNA, Inorg. Chim. Acta 157 (2) (1989) 271–281.
[38] D.K. Jangir, G. Tyagi, R. Mehrotra, S. Kundu, Carboplatin intercalation with calf thymus DNA: a FTIR spectroscopic approach, J. Mol. Str. 969 (1–3) (2010) 126–129.
[39] S. Agarwal, D.K. Jangir, P. Singh, R. Mehrotra, Spectroscopic analysis of the interaction of lomustine with calf thymus DNA, J. Photochem. Photobiol. B Biol. 130 (2014) 281–286.
[40] S. Mallick, P. Ghosh, S.K. Samanta, S. Kinra, B.C. Pal, A. Gomes, J.R. Vedasiromoni, Corchorusin-D, a saikosaponin-like compound isolated from *Corchorus acutangulus Lam.*, targets mitochondrial apoptotic pathways in leukemic cell lines (HL-60 and U937), Cancer Chem. Pharmacol. 66 (4) (2010) 709–719.
[41] C. Bohne, K. Faulhaber, B. Giese, A. Häfner, A. Hofmann, H. Ihmels, A.K. Kohler, S. Pera, F. Schneider, M.A. Sheepwash, Studies on the mechanism of the photo-induced DNA damage in the presence of acridizinium salts-involvement of singlet oxygen and an unusual source for hydroxyl radicals, J Am. Chem. Soc. 127 (1) (2005) 76–85.
[42] P. Basu, G.S. Kumar, Elucidation of the DNA binding specificity of the natural plant alkaloid chelerythrine: a biophysical approach, J. Photchem. Photobiol. B Biol. 138 (2014) 282–292.
[43] R. O'Brien, I. Haq, J.E. Ladbury, Applications of biocalorimetry: binding, stability and enzyme kinetics, in: M. Doyle (Ed.), Biocalorimetry, West Sussex, Wiley John and Sons Ltd., England, 2004, pp. 3–253.
[44] A.A. Saboury, M.S. Atri, M.H. Sanati, A.A. Moosavi-Movahedi, G.H. Hakimelahi, M.A. Sadeghi, Thermodynamic study on the interaction between magnesium ion and human growth hormone, Biopol. 81 (2) (2006) 120–126.
[45] N.J. Buurma, I. Haq, Advances in the analysis of isothermal titration calorimetry data for ligand-DNA interactions, Methods 42 (2) (2007) 162–172.
[46] M. Yang, K. Wang, C.B. Zang, B.H. Wang, Y.M. Zang, Binding of carboline derivatives to calf thymus DNA-determination of binding mode and binding strength, J Chinese Pharm Sci. 3 (1) (1994) 51–58.
[47] W. Du, B. Wang, Z. Li, Interaction of harmine with oligonucleotide $d(GTGCAC)_2$, Thermochemica Acta. 416 (1) (2014) 59–63.
[48] J.B. Chaires, A thermodynamic signature for drug-DNA binding mode, Arch. Biochem. Biophys. 453 (1) (2006) 26–31.
[49] M.M. Islam, P. Pandya, S. Roy Chowdhury, S. Kumar, G.S. Kumar, Binding of DNA-binding alkaloids berberine and palmatine to tRNA and comparison to ethidium: spectroscopic and molecular modeling studies, J. Mol. Str. 891 (2008) 498–507.
[50] A.H. Wyllie, The genetic regulation of apoptosis, Cur. Op. Gene. Dev. 5 (1) (1995) 97–104.
[51] T.L. Deckwerth, R.M. Easton, C.M. Knudson, S.J. Korsmeyer, E.M. Johnson, Placement of the BCL_2 family member BAX in the death pathway of sympathetic neurons activated by trophic factor deprivation, Exp. Neurol. 152 (1998) 150–162.
[52] T.J. Lindsten, A. Golden, W.X. Zong, J. Minarcik, M.H. Harris, C.B. Thompson, The proapoptotic activities of Bax and Bak limit the size of the neural stem cell pool, J. Neurosci. 23 (35) (2003) 11112–11119.
[53] A.L. Edinger, C.B. Thompson, Death by design: apoptosis, necrosis and autophagy, Cur. Opin. Cell Biol. 16 (6) (2004) 663–669.
[54] R. Cao, W. Peng, H. Chen, Y. Ma, X. Liu, X. Hou, H. Guan, A. Xu, DNA binding properties of 9-substituted harmine derivatives, Biochem. Biophys. Res. Commun. 338 (3) (2005) 1557–1563.
[55] W. Luo, J. Liu, J. Li, D. Zhang, M. Liu, J.A. Addo, S. Patil, L. Zhang, J. Yu, J.K. Buolamwini, J. Chen, C. Huang, Anti-cancer effects of JKA97 are associated with its induction of cell apoptosis via a Bax-dependent and p53-independent pathway, J. Biol. Chem. 283 (2008) 8624–8633.
[56] J. Zhang, Y. Li, G. Liang, R. Cao, P. Zhao, W. Jiang, Q. Ma, H. Yi, Z. Li, J. Jiang, J. Wu, Y. Wang, S. Si, DH166, a beta-carboline derivative, inhibits the kinase activity of PLK1, Cancer Biol. Therapy 8 (24) (2009) 2374–2383.
[57] G. Zachos, D.A. Spandidos, Expression of ras proto-oncogenes: regulation and implications in the development of human tumors, Critical Rev. Oncol. Hematol. 26 (2) (1997) 65–75.
[58] A. Tamaki, C. Ierano, G. Szakacs, R.W. Robey, S.E. Bates, Controversial role of ABC transporters in clinical oncology, Essays Biochem. 50 (1) (2011) 209–232.
[59] A.J. Colquhoun, N.A. Venier, A.D. Vandersluis, R. Besla, L.M. Sugar, A. Kiss, N.E. Fleshner, M. Pollak, L.H. Klotz, V. Venkateswaran, Metformin enhances the antiproliferative and apoptotic effect of bicalutamide in prostate cancer, Prostate Cancer Prostatic Dis. 15 (4) (2012) 346–352.
[60] D.L. Bemis, J.L. Capodice, M. Desai, A.E. Katz, R. Buttyan, Beta-carboline alkaloid-enriched extract from the amazonian rain forest tree pao pereira suppresses prostate cancer cells, J. Soc. Integr. Oncol. 7 (2) (2009) 59–65.
[61] M.A.M. El Gendy, A.A. Soshilov, Harmaline and harmalol inhibit the carcinogen-activating enzyme CYP1A1 via transcriptional and posttranslational mechanisms, Food Chem. Toxicol. 50 (2) (2012) 353–362.
[62] F. Lamchouri, M. Zemzami, A. Jossang, A. Settaf, Z.H. Israili, B. Lyoussi, Cytotoxicity of alkaloids isolated from Peganum harmala seeds, Pak. J. Pharm. Sci. 26 (4) (2013) 699–706.
[63] S.S.H. Tehrani, S.H.S. Shabani, S.T. Enferadi, Z. Rabiei, Growth inhibitory impact of *Peganum harmala* L. on two breast cancer cell lines, Iranian, J Biotech. 12 (1) (2014) 1–7.
[64] S.H.S. Shabania, S.S.H. Tehrania, Z. Rabieia, S.T. Enferadia, G.P. Vannozzib, Peganum harmala L'.s anti-growth effect on a breast cancer cell line, Biotech. Rep. 8 (2015) 138–143.
[65] X. Li, B. Bai, L. Liu, P. Ma, L. Kong, J. Yan, J. Zhang, Z. Ye, H. Zhou, B. Mao, H. Zhu, Y. Li, Novel β-carbolines against colorectal cancer cell growth via inhibition of Wnt/β-catenin signaling, Cell Death Dis. 15033 (1) (2015) 1–9.
[66] H.C. Chen, W.T. Heish, W.C. Chang, J.G. Chung, Aloe-emodin induced *in vitro* G2/M arrest of cell cycle in human promyelocytic leukemia HL60 cells, Food Chem. Toxi. 42 (8) (2004) 1251–1257.
[67] L.V. Li, H.J. Dai, M. Ye, S.L. Wang, X.J. Xiao, J. Zheng, H.Y. Chen, Y.H. Luo, J. Liu, Lycorine induces cell-cycle arrest in the G0/G1 phase in K562 cells via HDAC inhibition, Cancer cell Int. 12 (1) (2012) 12–49.
[68] M. Schuler, E.B. Wetzel, J.C. Goldstein, P. Fitzgerald, D.R. Green, p53 induces apoptosis by caspase activation through mitochondrial cytochrome c release, J. Biol. Chem. 275 (10) (2000) 7337–7342.
[69] J. Das, S. Das, A. Samadder, K. Bhadra, A.R. Khuda-Bukhsh, Poly (lactide-co-

glycolide) encapsulated extract of Phytolacca decandra demonstrates better intervention against induced lung adenocarcinoma in mice and on A549 cells, Eur. J. Pharma. Sci. 47 (2) (2012) 313–324.
[70] S. Saha, S. Sikdar, A. Mukherjee, K. Bhadra, N. Boujedainic, A.R. Khuda-Bukhsh, Ethanolic extract of the Goldenseal, *Hydrastis canadensis*, hasdemonstrable chemopreventive effects on HeLa cells *in vitro*: Drug–DNA interaction with calf thymus DNA as target, Envn. Toxl. Pharm. 36 (1) (2013) 204–214.
[71] Y. Yokomori, D.J. Hodgson, Guanidinium-carboxylate interactions II Crystal structures of methylguanidinium benzylhydrogenmalonate, methylguanidinium ethylhydrogenmalonate and methylguanidinium sulfate, Chem. Biol. Drug Desg. 31 (3) (1988) 289–298.
[72] P.A. Wender, D.J. Mitchell, K. Pattabiraman, E.T. Pelkey, L. Steinman, J.B. Rothbard, The design, synthesis, and evaluation of molecules that enable or enhance cellular uptake: peptoid molecular transporters, PNAS 97 (24) (2000) 13003–13008.
[73] R.J.T. Houk, S.L. Tobey, E.V. Anslyn, Abiotic guanidinium receptors for anion molecular recognition and sensing, Top. Curr. Chem. 255 (2005) 199–229.
[74] E. Waxselblatt, J.D. Esko, Y. Tor, On guanidinium and cellular uptake, J. Org. Chem. 79 (15) (2014) 6766–6774.